

**INVESTIGATION OF SWIRL FLOWS
APPLIED TO THE OIL AND GAS INDUSTRY**

A Thesis

by

MEHER SURENDRA RAVURI VENKATA KRISHNA

Submitted to the Office of Graduate Studies of
Texas A&M University
in partial fulfillment of the requirements for the degree of

MASTER OF SCIENCE

May 2009

Major Subject: Petroleum Engineering

**INVESTIGATION OF SWIRL FLOWS
APPLIED TO THE OIL AND GAS INDUSTRY**

A Thesis

by

MEHER SURENDRA RAVURI VENKATA KRISHNA

Submitted to the Office of Graduate Studies of
Texas A&M University
in partial fulfillment of the requirements for the degree of

MASTER OF SCIENCE

Approved by:

Co-Chairs of Committee,	Gioia Falcone
	Catalin Teodoriu
Committee Members,	Hamn-Ching Chen
Head of Department,	Stephen A. Holditch

May 2009

Major Subject: Petroleum Engineering

ABSTRACT

Investigation of Swirl Flows Applied to the Oil and Gas Industry. (May 2009)

Meher Surendra Ravuri Venkata Krishna, B.Tech. Jawaharlal Nehru Technical
University

Co-Chairs of Advisory Committee: Dr. Gioia Falcone
Dr. Catalin Teodoriu

Understanding how swirl flows can be applied to processes in the oil and gas industry and how problems might hinder them, are the focus of this thesis. Three application areas were identified: wet gas metering, liquid loading in gas wells and erosion at pipe bends due to sand transport. For all three areas, Computational Fluid Dynamics (CFD) simulations were performed. Where available, experimental data were used to validate the CFD results. As a part of this project, a new test loop was conceived for the investigation of sand erosion in pipes.

The results obtained from CFD simulations of two-phase (air-water) flow through a pipe with a swirl-inducing device show that generating swirl flow leads to separation of the phases and creates distinct flow patterns within the pipe. This effect can be used in each of the three application areas of interest.

For the wet gas metering application, a chart was generated, which suggests the location of maximum liquid deposition downstream of the swirling device used in the ANUMET

meter. This will allow taking pressure and phase fraction measurements (from which the liquid flow rate can be determined) where they are most representative of the flow pattern assumed for the ANUMET calculation algorithms.

For the liquid loading application, which was taken as an upscaling of the dimensions investigated for the wet gas metering application, the main focus was on the liquid hold-up. This parameter is defined as the ratio of the flowing area occupied by liquid to the total area. Results obtained with CFD simulations showed that as the water rate increases, the liquid hold-up increases, implying a more effective liquid removal. Thus, it was concluded that the introduction of a swirler can help unload liquid from a gas well, although no investigation was carried out on the persistence of the swirl motion downstream of the device.

For the third and final application, the erosion at pipe bends due to sand transport, the main focus was to check the erosion rate on the pipe wall with and without the introduction of a swirler. The erosion rate was predicted by CFD simulations. The flow that was investigated consisted of a liquid phase with solid particles suspended in it. The CFD results showed a significant reduction in erosion rate at the pipe walls when the swirler was introduced, which could translate into an extended working life for the pipe. An extensive literature review performed on this topic, complemented by the CFD simulations, showed the need for a dedicated multiphase test loop for the investigation of

sand erosion in horizontal pipes and at bends. The design of a facility of this type is included in this thesis.

The results obtained with this work are very encouraging and provide a broad perspective of applications of swirl flows and CFD for the oil and gas industry.

DEDICATION

I dedicate this thesis to my Mother and my Sister

ACKNOWLEDGEMENTS

I would like to express my sincere gratitude to my advisors Dr. Gioia Falcone and Dr. Catalin Teodoriu for giving me the opportunity to be a part of their team and this project and for their encouragement to learn and to provide meaningful results. Their knowledge and suggestions were fundamental throughout this work.

Thanks also go to the gas well unloading group: He Zhang, Gopi Chava, Juan Fernandez, Han-Young Park and Fouad Solomon for being such a great team to work with. I would also like to thank the department, faculty, and staff for making my time at Texas A&M University a great experience.

Thanks to Dr. Hamn-Ching Chen for serving on my committee. Finally, thanks to the Crisman Institute at the Department of Petroleum Engineering at Texas A&M University for the financial support.

TABLE OF CONTENTS

	Page
ABSTRACT	iii
DEDICATION	vi
ACKNOWLEDGEMENTS	vii
TABLE OF CONTENTS	viii
LIST OF FIGURES	xi
LIST OF TABLES	xv
 CHAPTER	
I INTRODUCTION.....	1
1.1. Research Objectives	1
1.2. Problem Description	2
1.3. Structure of Thesis	4
II FUNDAMENTALS OF SWIRL FLOW	5
2.1. Principles of Swirling Flow.....	6
2.2. Static and Dynamic Pressures	10
2.3. Pressure Drop	11
2.4. Applications of Centrifugal Separators	12
III REVIEW OF PROCESSES WHERE SWIRL FLOWS CAN BE APPLIED	14
3.1. Liquid Loading.....	14
3.1.1. Liquid Loading in High Gas Fraction Wells.....	14
3.1.2. Problems Caused by Liquid Loading.....	16
3.1.3. Solution to Liquid Loading.....	18

CHAPTER	Page
3.1.4. Flow Conditioning	19
3.2. Erosion in Pipes.....	25
3.2.1. How Does Erosion Occur?.....	25
3.2.2. Critical Depositional Velocity	29
3.2.3. Application of Swirlers to Reduce Erosion	31
3.3. Wet Gas Metering	33
3.3.1. Definition of Wet Gas.....	33
3.3.2. Problems Associated with Wet Gas Metering	35
3.3.3. ANUMET	36
IV COMPUTATIONAL FLUID DYNAMICS (CFD)	40
4.1. Introduction	41
4.2 Flow Modeling Techniques.....	49
4.2.1. Lagrangian Description.....	49
4.2.2. Eulerian Description	51
4.3. Governing Equations.....	52
4.4. Homogeneous Model	54
4.5. Inhomogeneous Model.....	55
4.5.1. The Particle Model.....	56
4.5.2. The Mixture Model.....	57
4.5.3. The Free Surface Model.....	58
4.6. Simulating Turbulence	58
4.7. Erosion Model	63
4.8. Other Applications of CFD	64
V NUMERICAL INVESTIGATION OF SWIRL FLOWS	66
5.1. ANUMET Validation.....	66
5.2. Liquid Loading.....	70
5.3. Erosion in Pipes	71

CHAPTER	Page
VI RESULTS.....	72
6.1. ANUMET Validation.....	72
6.1.1. Maximum Liquid Deposition.....	77
6.1.2. Pressure and Density.....	79
6.2. Liquid Loading.....	85
6.3. Erosion at Pipe Bends Due to Sand Transport.....	89
6.4. Multiphase Flow Loop.....	91
VII CONCLUSIONS AND RECOMMENDATIONS.....	98
NOMENCLATURE.....	100
REFERENCES	102
VITA	104

LIST OF FIGURES

FIGURE	Page
2.1 A particle in swirl motion	5
2.2 Forced vortex flow	6
2.3 Velocity distribution in free vortex flow	7
2.4 A fluid element in a swirling flow, two different points of view	8
2.5 Detail of a rotating fluid element in a rotating coordinate system	8
2.6 Sketch showing the two ideal vortex flows, and the tangential velocity distribution in a Rankine vortex	9
3.1 Change in key properties as time progresses	15
3.2 Distribution of phases after flow past swirler	21
3.3 No-flow boundary at the edge of the gas stream and along the pipe wall	21
3.4 Vortex tool.....	22
3.5 Change in production variables before and after introduction of tool.....	23
3.6 Auger tool.....	24
3.7 Wear hot spots and settling of slurries	26
3.8 Visualization of erosion rate on pipe wall.....	27
3.9 Pipe bends which are potential areas for erosion	28
3.10 Gravitation and fluid-flow forces acting on a particle near the bottom of a horizontal pipe.....	30

FIGURE	Page
3.11 Flow before and after introduction of swirler	32
3.12 Swirl flow boiler tube used in swirl generation	33
3.13 Classification of reservoir fluids	35
3.14 The ANUMET wet gas metering concept.....	38
3.15 Droplet separation efficiency at 0, 3 and 11 diameters downstream of a fish-tail twisted tape device	39
4.1 Flowchart depicting methodology adopted in a CFD process	43
4.2 Geometric model of a tank	45
4.3 Boundary conditions for the tank.....	46
4.4 Numerical grid for the tank model.....	48
4.5 Plot showing air velocity distribution in the tank	48
4.6 Change in control volume	49
4.7 Particle tracks of sand particles in a pipe bend obtained from CFD simulation which incorporated the Lagrangian approach	50
4.8 Eulerian approach.....	51
5.1 Flow chart depicting the methodology adopted for the ANUMET Validation process	67
5.2 Actual ANUMET geometry as modeled with CFX before modifications.....	69
5.3 Simplified ANUMET geometry as modeled with CFX.....	69
5.4 Inflated boundary at pipe wall as modeled with CFX	70
6.1 Values for density- Homogeneous model	73

FIGURE	Page
6.2 Separation of phases. Water is at concentrated along the pipe wall (red) resulting in a fluid film	75
6.3 Fluid film (red band) at the pipe wall.....	75
6.4 Density ranges predicted by the free surface model	76
6.5 Maximum liquid deposition	77
6.6 Graph showing range of maximum liquid deposition for a given volume fraction of water	79
6.7 5 sectional planes chosen along the length of the pipe.....	81
6.8 6 lines chosen along the length of the pipe	81
6.9 Sectional plane chosen along the length of the pipe	82
6.10 Pressure vs. length.....	83
6.11 Fluid pressure contours at the 5 cross-sectional planes.....	84
6.12 Pressure along the horizontal plane.....	84
6.13 Density along the 5 sectional planes	85
6.14 Water superficial velocity on 5 sectional planes	86
6.15 Changes in air superficial velocity along the pipe	87
6.16 Air superficial velocity along the pipe	89
6.17 Erosion rate before and after introduction of swirler	90
6.18 Pressure drop (2.8 psi) in 3 inch diameter pipe.....	91
6.19 Pressure drop (3 psi) in 2.5 inch diameter pipe.....	92
6.20 Pressure drop (10 psi) in 2 inch diameter pipe.....	93
6.21 Flow loop.....	94

FIGURE	Page
6.22 Instrumentation currently used.....	95
6.23 Air and water inlet.....	96
6.24 Water tank	97

LIST OF TABLES

TABLE	Page
6.1 Parameters used in the simulation	72
6.2 Input parameters for simulations	78
6.3 Distances of each plane from the inlet plane.....	80
6.4 Flow rate data used for simulations in order to check the relation between liquid-hold up and water rate	88

CHAPTER I

INTRODUCTION

1.1 Research Objectives

The main objective of this work is to identify processes in the oil and gas industry where swirl flows can be introduced to mitigate operational problems and optimize production. Following an extensive literature review, three areas were identified where there was enough potential to investigate the effects of swirl flow. These are: wet gas metering, liquid loading in gas wells and erosion at bends due to sand transport. In order to investigate the effects of introducing swirl flow Computational Fluid Dynamics (CFD) was used. The commercial software adopted for this work was CFX 10.0 by ANSYS.

For the investigation of swirl flow in wet gas metering applications, the experimental data obtained by Falcone et al. (2003) during the development of the ANUMET flow meter were used for the CFD simulations. In this meter, measurements are taken downstream of a twisted tape device to determine the liquid rate in a two-phase flow. The results of the CFD runs were captured in a chart showing the location of the maximum liquid deposition downstream of the swirler.

This thesis follows the form and style of the *SPE Journal*.

This will allow taking pressure and phase fraction measurements (from which the liquid flow rate can be determined) where they are most representative of the flow pattern assumed for the ANUMET calculation algorithms. For the liquid loading application, the main objective was to verify whether introducing a swirler can help delay the onset of liquid loading.

The use of swirl flow to reduce erosion at pipe bends was investigated in two ways. The first step was to compare the erosion rates on the pipe walls with and without the swirler by means of CFD simulations. The second step was to design a dedicated multiphase test loop for the investigation of sand erosion in horizontal pipes and at bends. Given the physical constraints of the laboratory space available for the loop (in the Petroleum Engineering department at Texas A&M University) and the results of the CFD simulations, the following specifications were recommended for the facility: total length of horizontal test section – 12ft; pipe material – Perspex (to allow visual observation of the flow and the use of high-speed or Particle Image Velocimetry cameras); pipe diameter – 3”.

1.2 Problem Description

In what follows, the three above-mentioned application areas are briefly discussed:

- a) Liquid Loading: liquid loading occurs when the flowing gas is no longer capable of lifting the liquids to the surface. The liquids fall back into the tubing, choking

the flow and eventually killing the well. The major focus of this work is to check if the introduction of a swirl-inducing device in the tubing can help mitigate the impact of liquid loading or delay its onset. Previous work carried out at Texas A&M tested two of these tools for downhole application (Bose in 2007 and Scott S.L et al in 2003). These studies did not focus on the actual flow dynamics of the problem and did not attempt CFD modeling.

- b) Wet gas Metering: when using the ANUMET meter (Falcone et al., 2003) to predict the liquid rate in a two-phase flow it is essential that pressure and phase fraction measurements are taken where there is maximum liquid deposition downstream of the swirling device. Experimental results suggest that, although the point of minimum entrained fraction (i.e. the point that corresponds to the peak of the film thickness) increases with increasing air flow rate and decreases with increasing water flow rate, an optimal location can be considered to be that at approximately ten diameters downstream the outlet of the swirler (Falcone et al., 2003). CFD simulations allow to model where maximum deposition occurs.
- c) Erosion in pipes: Erosion occurs in pipes and at bends due to sand and particle transport. Experimental results and analytical models for erosion in pipes are available in the public domain. However, the specific effects of swirl flow have been fully investigated and CFD can prove invaluable in complementing the current knowledge in this area. Experimental data from a dedicated test loop are needed to calibrate and validate CFD models for the case of swirl flow, and hence the facility design effort included in this study.

1.3 Structure of Thesis

Chapter I introduces the three application areas addressed in this work. Chapter II is a description of the processes where swirl flows can be applied to mitigate specific problems, including a review of previous work carried out in these areas. Chapter III reviews the fundamental principles of swirl flows. Chapter IV is an introduction to CFD, including the models available within the commercial software package used for this work and other models that can be used to mimic the flow process investigated in this framework. Chapter V describes the methodology adopted in this study for each of the three application areas under investigation. Chapter VI presents the results from CFD simulations. Chapter VII presents the conclusions and recommendations from this work.

CHAPTER II

FUNDAMENTALS OF SWIRL FLOW

A particle is said to be in swirling flow or motion (as shown in fig 2.1) if it has a rotational velocity along with a linear velocity component. The path followed by the particle would be similar to a helix or spiral. The main advantage of swirl flows is that we can use the rotational component and modify the flow process to our advantage. This approach is extensively used in the hydrocyclones and gas cyclones used in the upstream equipment of the production facilities.

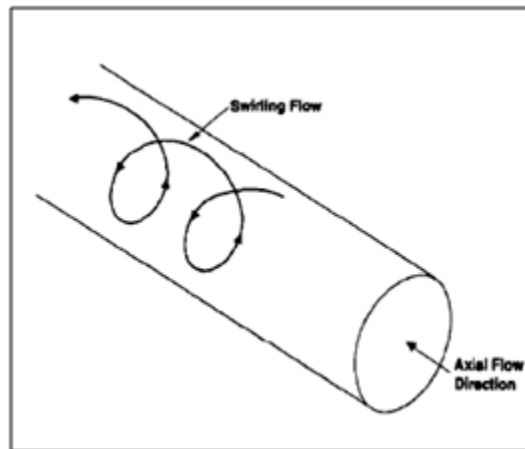


Fig 2.1- A particle in swirl motion

2.1 Principles of Swirling Flow

Swirling flow occurs in different types of equipment, such as cyclones, hydrocyclones, spray dryers and vortex burners which are a major part of process equipment in the oil and gas industry. It is also the basis for the operation of foam-breaking or ‘defoaming’ separators that have received significant industrial attention in recent years.

There are two types of ideal swirling flows:

- a) Forced vortex flow, this kind of vortex is also called irrotational vortex or a flywheel vortex (figure 2.2). The tangential velocity (v) varies inversely as the distance from the center (r) so the angular velocity is constant (equation 2.1). The tangential velocity distribution would be same as a rotating solid body.

$$v/r = \text{constant} \dots \dots \dots (2.1)$$

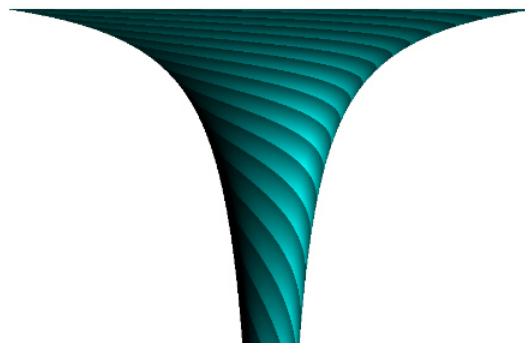


Fig 2.2 -Forced vortex flow (www.nct.anth.org.uk/path.htm)

- b) Free vortex flow, this kind of vortex is also called rotational vortex or potential vortex. The product of tangential velocity (v) and the distance from the center (r)

is a constant (equation 2.2). The tangential velocity in such a swirl is such that the moment-of-momentum of fluid elements is the same at all radii or in simple terms as the radius increases the tangential velocity decreases (figure 2.3).

$$vr = \text{constant} \dots \dots \dots (2.2)$$

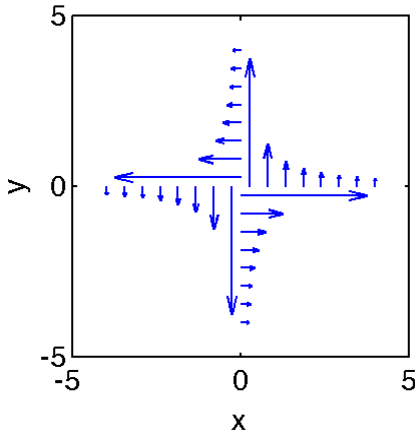


Fig 2.3- Velocity distribution in free vortex flow

(www.me.pdx.edu/~gerry/class/ME322/notes/)

The tangential velocity distribution in real swirling flows is intermediate between these two extremes. Figure 2.4 depicts the forces acting on a fluid element from two different coordinate systems. Newton's equations of motion can be applied only in a non accelerating coordinate system. Since most of the physical systems are accelerating or rotating a "pseudo force" like the "centrifugal force" in order to apply or preserve the equation of motion. We say "non-physical" because, in a rotating coordinate system, it is not possible to identify a physical object which produces the force needed to satisfy Newton's laws of motion.

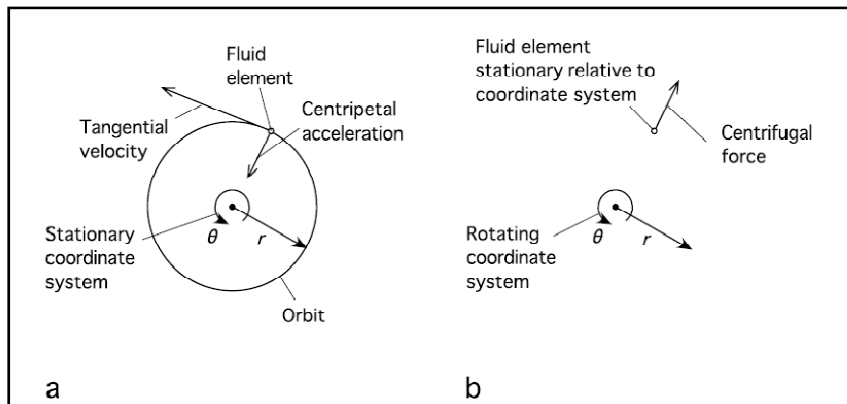


Fig 2.4 - A fluid element in a swirling flow, from two different points of view

(Hoffman and Stein, 2007)

Real forces always occur in pairs. For a fluid element (as opposed to a solid or liquid particle), the “centrifugal force” is balanced by a force created by a gradient in the static pressure. This pressure gradient acting over the surface of the particle, acts toward the axis of rotation and keeps the element in its path (Figure 2.5). The pressure in a swirling flow increases with the distance from the axis of rotation.

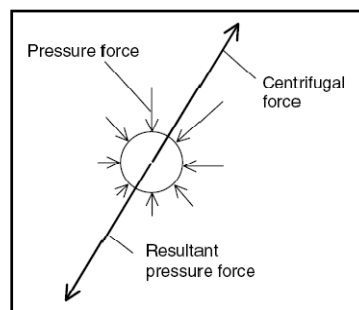


Fig 2.5- Detail of a rotating fluid element in a rotating coordinate system

(Hoffman and Stein, 2007)

A real fluid will have some finite viscosity, which will cause transfer of moment-of-momentum between layers at different radii. An additional transport of moment-of-momentum will be caused by any turbulence present, due to exchange of fluid elements between the layers. A real swirling flow normally has a core of near solid-body rotation surrounded by a region of near loss-free rotation as sketched in Fig.2.6 This is called a 'Rankine vortex'.

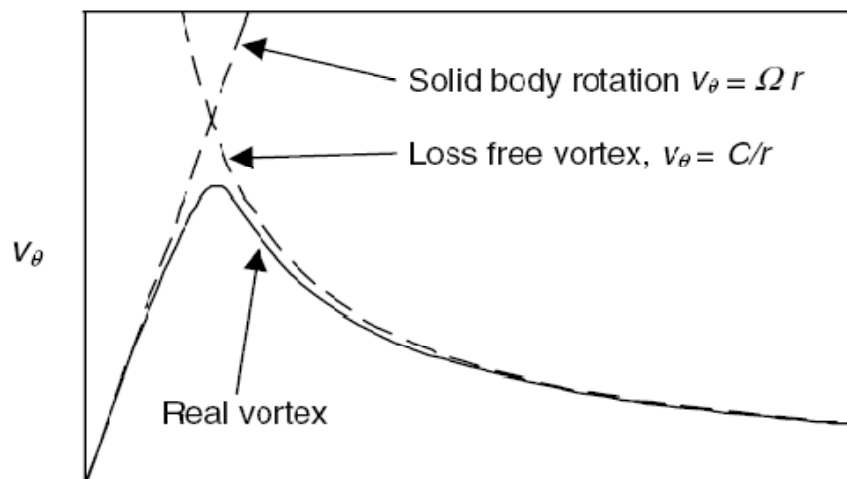


Fig 2.6- Sketch showing the two ideal vortex flows, and the tangential velocity distribution in a Rankine vortex (Hoffman and Stein, 2007)

2.2 Static and Dynamic Pressures

The flow and pressure distribution in swirl flows depends on static and dynamic particle motion pressures. The Bernoulli equation for steady flow of a frictionless, constant density fluid along a streamline is

$$P + \rho gh + 1/2 \rho v^2 = \text{Constant} \dots \dots \dots (2.3)$$

' P ' is the static pressure and ' $\rho gh + 1/2 \rho v^2$ ' is the dynamic pressure. The first and third terms on the left-hand side of the equation are called 'Velocity Head'. This equation shows that static and dynamic pressures can be interchanged in the flow field. In areas where the velocity is high, the static pressure will be low and vice versa.

This is the principle used in many flow meters, for instance pitot tubes and venturi meters. This interdependence between static and dynamic pressure gains significant importance when dealing with swirling flows. The left-hand side of the Eq. 2.3 is sometimes called 'Bernoulli's trinomial'.

The second term is unimportant relative to the two others when discussing cyclones and swirl tubes, since the fluid density is relatively low, and height differences not very large. In reality the fluid is not frictionless. Frictional dissipation of mechanical energy causes Bernoulli's trinomial to decrease in the flow direction, i.e. the trinomial is no longer constant, but decreases along a streamline.

2.3 Pressure Drop

The normal procedure for measuring a pressure drop in the process industry is to measure the static pressure at the wall in the upstream and downstream piping. This is complicated in swirl flows because of two reasons.

1. Firstly the swirl causes the static pressure at the wall to be higher than the cross-sectional average.
2. Secondly dynamic pressure is stored in the swirling motion.

In order to calculate the total pressure we need the sum of the static and dynamic pressure drops.

The pressure drop over a cyclone is mainly due to the following three losses:

1. losses in the entry,
2. losses in the separation space (the main cyclone body), and
3. Losses in the vortex finder.

The losses in the entry are often negligible compared to the other contributions, at least in tangential entry cyclones. For swirl tubes with inlet vanes little information is available, but if the vanes are properly contoured aerodynamically, the losses are generally small. The losses in the cyclone body are higher, but their main significance is in limiting the intensity of the swirl in the separation space. More frictional losses at the walls lead to a less intensive vortex. Such wall losses do not dominate the overall pressure drop. The losses in the vortex finder are the largest, in both through-flow and

reverse-flow tangential-inlet cyclones. Vortex finder losses may be an order of magnitude larger than the two other contributions.

For particle laden flow wall losses associated with frictional drag at the walls can become a significant contribution to the overall pressure loss which occurs at the expense of losses in the vortex core, and the vortex finder. The pressure drop over a cyclone (Δp) is proportional to or very close to being proportional to the square of the volumetric flowrate, as it is in all processing equipment with turbulent flow. To obtain a characteristic measure for pressure drop in a given cyclone, pressure drop is often reported in a dimensionless form known as the ‘Euler number’:

$$Eu = \Delta p / (0.5 \rho v_z^2) \dots \dots \dots (2.4)$$

V_z is the mean axial velocity in the body, i.e. the volumetric flow rate divided by the cross-sectional area of the cylindrical part of the body. It velocity used to define the Euler number is user dependent.

2.4 Applications of Centrifugal Separators

Cyclonic separation technology offers advantages such as lower weight and space savings for topsides and subsea applications. Inlet cyclones, demisting cyclones, and

stand-alone monocyklones are being considered more often in the process design. The following are the advantages of swirl technology/swirlers are:

1. Low capital investment and maintenance costs in most applications.
2. Very compact in most applications.
3. Can be used under extreme processing conditions, in particular at high.
4. Temperatures and pressures and with chemically aggressive feeds.
5. No moving parts.
6. Very robust.
7. Constant pressure drop.
8. Can be constructed from most any material suitable for the intended service including plate steel, casting metals, alloys, aluminum, plastics, ceramics, etc.
9. Can be equipped with erosion or corrosion resistant or 'particle repelling' type liners, such as Teflon.
10. Internal surfaces may be electropolished to help combat fouling.
11. Can be fabricated from plate metal or, in the case of smaller units, cast in molds.
12. Can, in some processes, handle sticky or tacky solids with proper liquid irrigation.
13. Can separate either solids or liquid particulates; sometimes both in combination with proper design.

CHAPTER III

REVIEW OF PROCESSES WHERE SWIRL FLOWS CAN BE APPLIED

After literature review three main three areas were selected. In this chapter each of these areas along with work done previously and the actual problem in each of these areas are discussed in detail.

3.1 Liquid Loading

3.1.1 Liquid Loading in High-Gas Fraction Wells

Generally natural gas production is associated with production of liquid hydrocarbons, water from formation and other liquids, very few wells produce completely dry gas. At the beginning of production or early life of the well there is enough drive or pressure from the reservoir which ensures that the velocity of the gas is high enough for all the fluids produced to reach the surface. As time goes on, gas production and reservoir pressure decrease consequently the velocity of the gas decreases. The flowing gas is no longer capable of lifting the liquid to surface. This triggers liquid accumulation in the wellbore, resulting in additional hydrostatic pressure that impairs the gas inflow from the reservoir. This gradual accumulation of fluids in the wellbore reduces production and will eventually kill the well.

If the reservoir pressure is low, the accumulated liquid may completely stop gas production. If the reservoir pressure is higher, liquid slugging or churning may occur in

the production system, although this intermittent flow response is a temporary feature, the well eventually dies.

The following diagram (Figure 3.1) shows the change in the key parameters of a producing well as time progresses pertinent to the liquid loading issue.

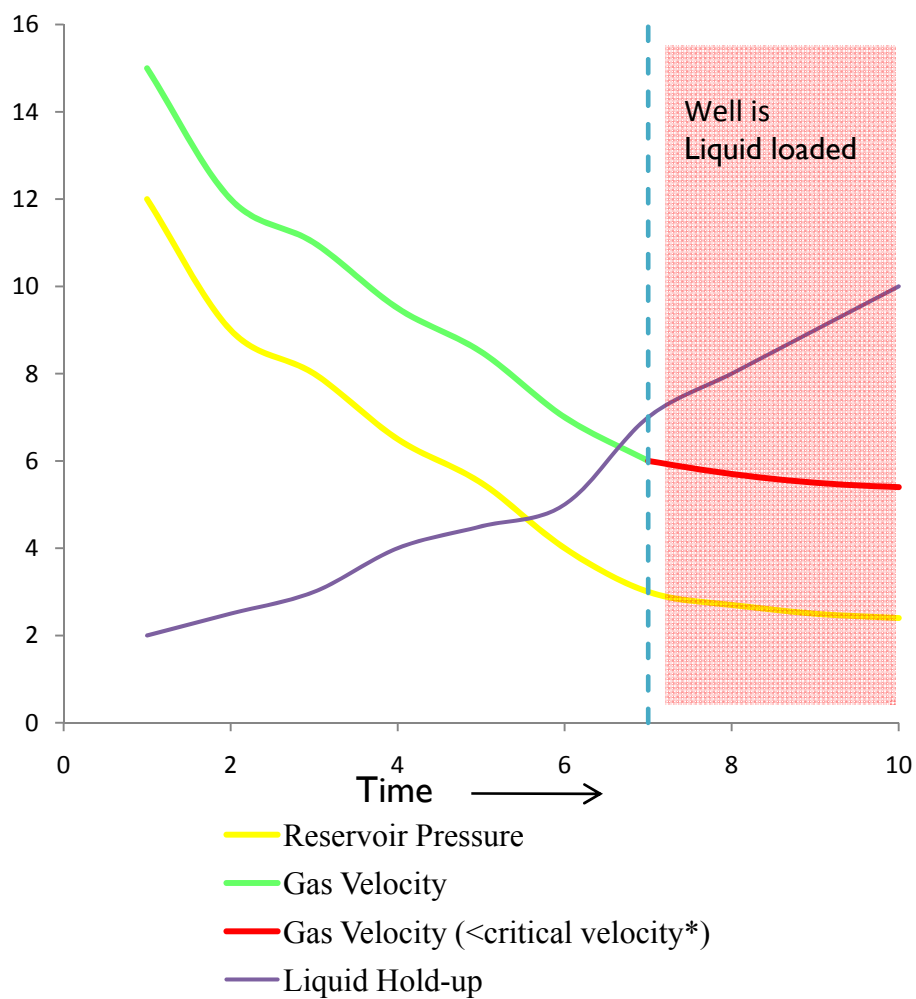


Fig 3.1- Change in key properties as time progresses

(This is a generic plot. It is not based on any specific data set)

* Critical Velocity is defined as the minimum velocity of the gas in the production tubing to ensure the liquids reach the surface. There are many underlying assumptions which define critical velocity for instance critical velocity is calculated assuming that water or liquid are in droplet phase.

The origin of the liquids in the gas stream could be any of the following.

1. Liquids produced directly into the wellbore from the reservoir.
2. Both hydrocarbons (Condensate) and water may condense from the gas stream as the temperature and pressure change during travel to the surface.
3. Fluids may come into the wellbore as a result of coning water from an underlying zone.
4. The fluids could be from an aquifer which initially provides pressure support but eventually would let fluids into the wellbore leading to liquid loading problems.

3.1.2 Problems Caused by Liquid Loading

Liquid loading can lead to erratic, slugging flow and to decreased production from the well. The well may eventually die if the liquids are not removed continuously, or the well may produce at a lower rate than possible.

If the gas rate is high enough to continually produce most or all of the liquids, the wellbore formation pressure and production rate will reach a stable equilibrium operating point. The well will produce at a rate that can be predicted by the reservoir inflow performance relationship (IPR) curve. If the gas rate is too low, the tubing pressure gradient becomes larger because of the liquid accumulation resulting in increased pressure on the formation.

As the backpressure on the formation increases, the production rate from the reservoir decreases and may drop below the critical rate. Critical rate is defined as the minimum flow rate of the gas to ensure the liquids reach the surface. If the gas rate drops below the critical rate more liquids will accumulate in the wellbore, and the increased hydrostatic pressure will reduce production or may kill the well.

Late in the life of the well, liquid may entirely fill the production tubing with the gas bubbling through the liquid to the surface. If it is observed that gas is being produced at a slow but steady rate, and no liquids are being produced at the surface it could be misinterpreted as a low gas producing well but not liquid loaded. This could be avoided by analyzing the production history of the well.

All gas wells that produce liquids irrespective of whether they are in a high or low permeability formations will eventually experience liquid loading with depleting reservoir pressure. Even wells with very high gas-liquid ratios (GLR) and small liquid

rates can load up if the gas velocity is low. This condition is typical of low permeability gas wells that produce at low gas rates and have low gas velocities in the tubing.

3.1.3 Solution to Liquid Loading

Several actions can be taken to reduce/remediate liquid loading. Although it would boil down to availability of proper equipment and cost to determine the optimum remedy depending on the reservoir pressure the following options is available.

1. Use nodal analysis method to evaluate the optimum tubing size to avoid future loading effects. In Nodal Analysis method we use multiphase flow correlations developed for the various components such as reservoir, well completion, and surface equipment systems to calculate the pressure loss associated with each component and to evaluate well performance under a variety of conditions.
2. Flow conditioning by introducing downhole tools in the production conduit is another option. These tools alter the flow pattern inside the pipe by generating swirls. This phenomenon is being investigated in this project.
3. Using Plunger lift is another option. Plunger lift is an intermittent artificial lift method that uses the energy of the reservoir to produce the liquids to the surface. A plunger is a free-traveling piston that fits within the production tubing and

depends on well pressure to rise and solely on gravity to return to the bottom of the well.

4. Using smaller size tubing would ensure a higher gas velocity so that the velocity in the tubing is maintained above the critical velocity for a longer time.
5. Dropping or injecting foam or soap sticks down the production conduit. The benefit of foam is that liquid is held in the bubble film and exposed to more surface area, resulting in less gas slippage and a low-density mixture.
6. Using submersible pumps which can be dropped into the tubing to drive the liquids to the surface is another option.
7. Reservoir flooding in order to provide additional pressure support is employed when the bounds of the reservoir are known.

3.1.4 Flow Conditioning

Flow conditioning refers to the process where the flow pattern inside the pipe is altered by various methods to ensure a flow pattern which is reflective of the flow conditions inside the pipe. This is particularly important in flow measurement.

Irregularities in the gas velocity profile, varying turbulence levels, swirl and any other fluid flow characteristics cause the meter to register flow different than that actually is in the pipe. This will cause the meter to differ from the original Calibration State.

Flow Conditioning refers to the process of artificially generating a reference, fully-developed flow profile and is essential for accurate measurement. Since the phenomenon of liquid loading depends on the kind of flow pattern in the pipe generating a favorable flow pattern or maintaining it would ensure production. There are commercially available Downhole tools which can be introduced into the wellbore so that they generate swirl patterns which deter liquid loading.

Working principle

The flow conditioning device creates two distinct flows. Spiral or helical flow is established along the outer periphery of the pipe which carries most or all of the liquid phase. The center of the pipe is occupied by a strong flow of gas phase (Figure 3.2). The efficiency of the swirler would depend on how much liquid is still entrained in the gas core.

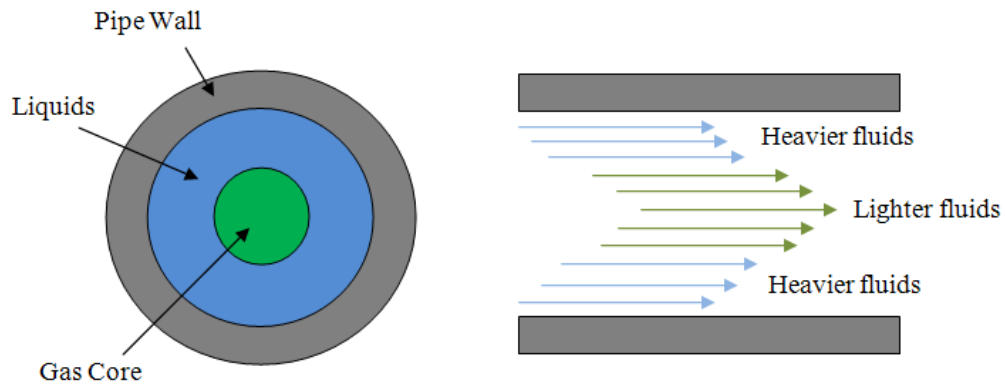


Fig 3.2- Distribution of phases after flow past swirler

The combined flow stream of gas and liquids on entering the tool is subjected to rapid spinning by the helical forces caused by the bluff body. The heavier fluid is moved to the pipe due to the centrifugal force. The gas starts moving centrally with the no-flow boundary (Figure 3.3) at the edge of the gas stream and along the pipe wall.

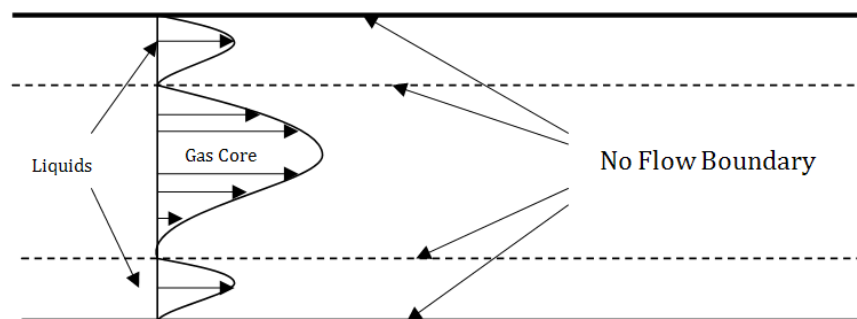


Fig 3.3- No-flow boundary at the edge of the gas stream
and along the pipe wall

This no flow boundary results in a lower differential velocity between the gas and the liquid, which lowers the shear force and frictional pressure. Reduction of this slip force between liquid droplets in the flow and the natural gas stream reduces amount of work performed by the natural gas and thus reducing the total pressure drop.

One such Downhole tool is the vortex tool. (Figure 3.4) field testing of this showed considerable changes in the field variables before and after introduction in a liquid loaded well (figure 3.5). This study showed some success as to the working of this Downhole tools.

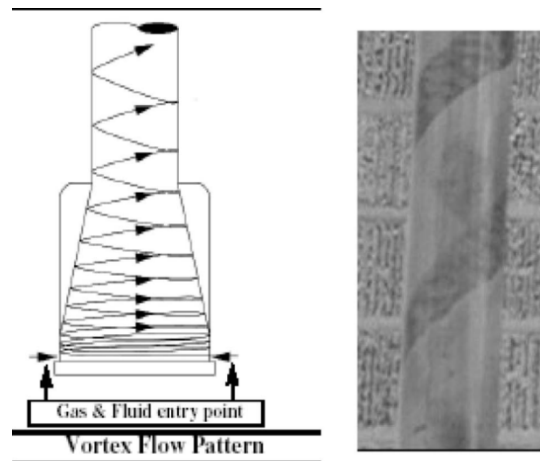


Fig 3.4- Vortex tool (Ali, Fehn and Scott- SPE 84136)

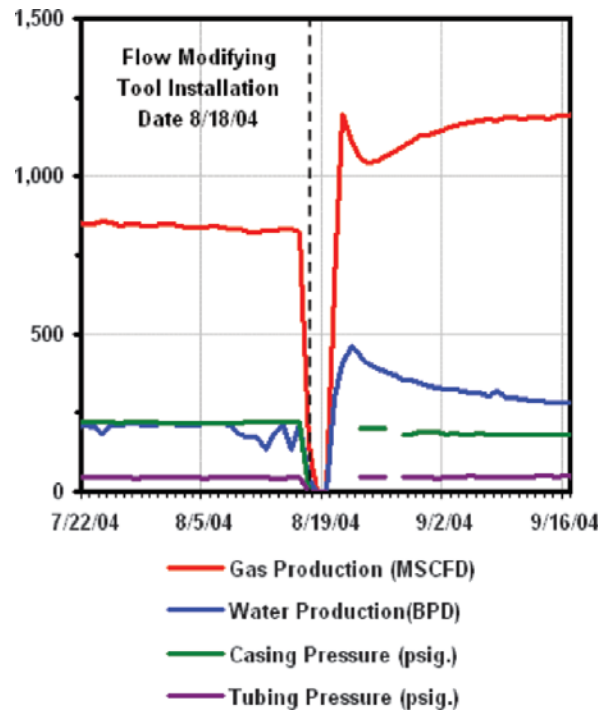


Fig 3.5 -Change in production variables before and after introduction of tool (Ali, Fehn and Scott ,2005)

The second such tool is the auger tool (figure 3.6). One such study conducted experiments using this tool in combination with foam (Bose .R, May, 2007). Introducing the auger tool into the wellbore did lower pressure drop, lower liquid hold up, reduce terminal velocity, and also the liquid unloading ability was enhanced but the best performance in the context of all the above parameters came with the auger tool used in combination with the surfactant foam.

Lower pressure drop resulted in higher recovery from the wells. The major drawback of using the auger tool was reduction in the operating envelope. Less quantity of water was handled in both the air-water and air-foam system.



Fig 3.6- Auger tool

The study aims to investigate the efficiency of the liquid separation at high gas fraction and to evaluate the persistence of the swirl downstream of the flow conditioning device. These features are essential to understand not only the efficiency of in-line separation devices used for gas metering purposes, but also that of Downhole tools for liquid unloading in gas wells. Laboratory tests/field installations carried out to date still do not confidently define the range of applicability for such tools. This is believed to be a consequence of the fact that the actual flow dynamics through the devices are still not

fully understood, and the relationship between tool geometry, flow rates, operating pressure, well geometry (length, diameter and orientation) and swirl persistence is yet to be proven.

3.2 Erosion in Pipes

Erosion mainly occurs when solid particulate matter is transported in pipes along with the essential production fluids. Sand production is a major problem in oil and gas production operations. Sand erosion due to sand production is a major issue. It causes loss of pipe wall thickness which leads to expensive failures and loss of production. Even if the amount of sand is less it can cause major erosion damage at high production velocities. Erosion damage causes downtime, loss of income and high repair costs. In the UK, a survey by the Department of Trade and Industry put the cost of erosion at around £20 million/annum. Costs can be as high as £500,000 for subsea replacements in the oil and gas industry. In extreme cases pipeline components are eroded away in months.

3.2.1 How Does Erosion Occur?

Pipes with a circular cross-section are the simple choice for piping applications. Their smooth interior makes no obstruction to encourage wear or excessive pressure loss. They are inexpensive to make and they are almost everywhere.

The low internal surface roughness of circular pipes encourages the settling of low-speed slurries. To avoid settling of particles in pipes designers specify a minimum speed to entrain the particles into the flow. This velocity is usually higher than the velocity just needed to transport slurry, as a result pumping is required and this increases the tendency of components to wear.

Bends are subject to maximum erosion because they absorb most of the momentum from particle which impinge on them. Impact between particles and bend walls can be at any angle between normal and parallel to the surface. These result in multiple erosion mechanisms which lead to cutting, deformation and ploughing wear. Figure 3.7 shows the mechanism of how erosion occurs at pipe bends. The direction of flow is indicated by the arrow in the figure. Particles are guided by bends and hence there is maximum erosion due to maximum contact. Figure 3.8 shows the erosion rate on the pipe wall for a generic case.

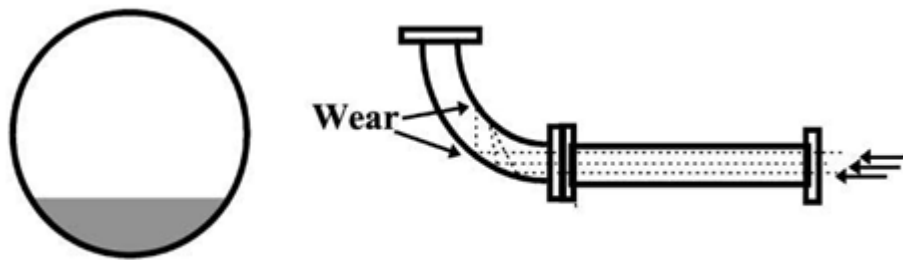


Fig 3.7- Wear hot spots (right) and settling of slurries (left)

(Wood, Jones, Miles, Ganeshalingam, 2001)

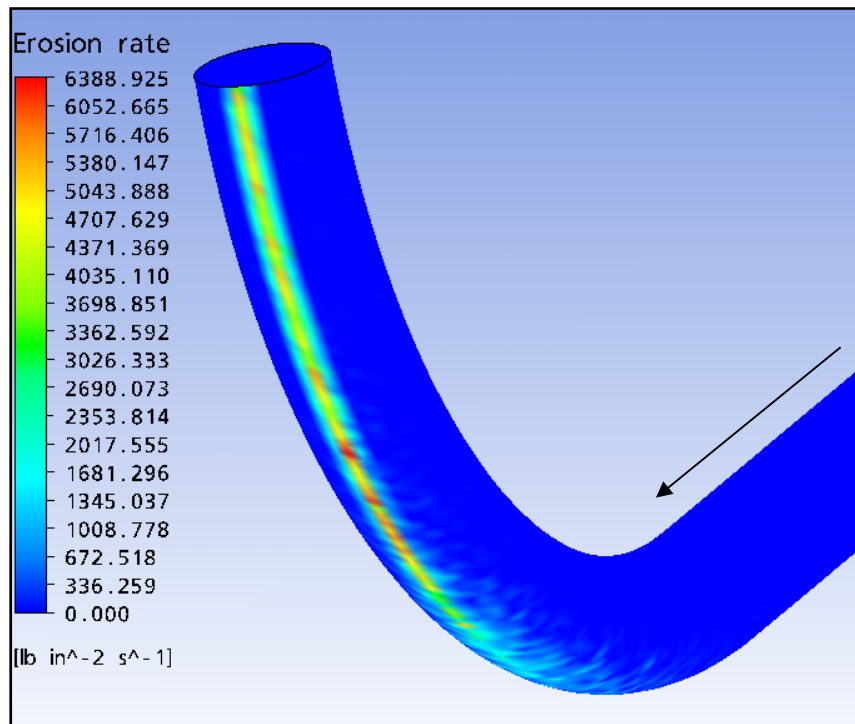


Fig 3.8- Visualization of erosion rate on pipe wall

The figure above shows results from a CFD simulation. This is to illustrate how we can view results using CFD.



Fig 3.9 - Pipe bends which are potential areas for erosion

Figure 3.9 shows actual pipework which can be potential candidates for erosion. The other problem with sand in pipes is that sand gets accumulated at the bend and as time passes it may eventually choke the flow resulting in decrease in flow velocity. As the reservoir pressure decreases and as time passes the amount of suspended particles travelling past the bend decrease. This results in accumulation of particles at the bend resulting in a blockage eventually choking the flow.

Apart from these reasons the other reasons for removing sand from production fluids are

1. Increased production capacity in the flow line.
2. Reduce the use of hydrate and corrosion inhibitors.
3. Standard instrumentation can be used for metering purposes if phases are separated.

3.2.2 Critical Depositional Velocity

During production or transportation we generally wish to avoid particles settling in the horizontal pipes either feeding or exiting the surface equipment. It is essential we know the minimum velocity required to prevent solid particles from settling and accumulating on the bottom of the piping. Wicks (1971) examined the forces acting on a particle resting at the bottom of a horizontal pipe such as lift, drag, buoyancy and gravity (similar to the principles outlined by White, 1940) and developed a very useful correlation for computing the minimum superficial pipe velocity V_S required to prevent a particle from stagnating along the bottom of the pipe. His equation may be expressed in the form

$$1 = \alpha V_S + \beta (V_S)^{2.5} \dots \dots \dots (3.1)$$

Where

$$\alpha = 10\mu / (\rho_p - \rho) * g * D_p \dots \dots \dots (3.2)$$

and

$$\beta = \frac{\rho^{1.5}}{100 (\rho_p - \rho) * g * \mu^{0.5} * D_p^{0.5}} \dots \dots \dots (3.3)$$

ρ	=	Density of fluid
ρ_p	=	Density of particle
g	=	Gravity
μ	=	Viscosity of the fluid
D_p	=	Diameter of the particle

Though/ Wicks' technique was originally derived for liquid-solid systems, it has been found that it can be applied to 'fluids' in general and is recommended for gas-solids systems in addition to liquid-solid systems.

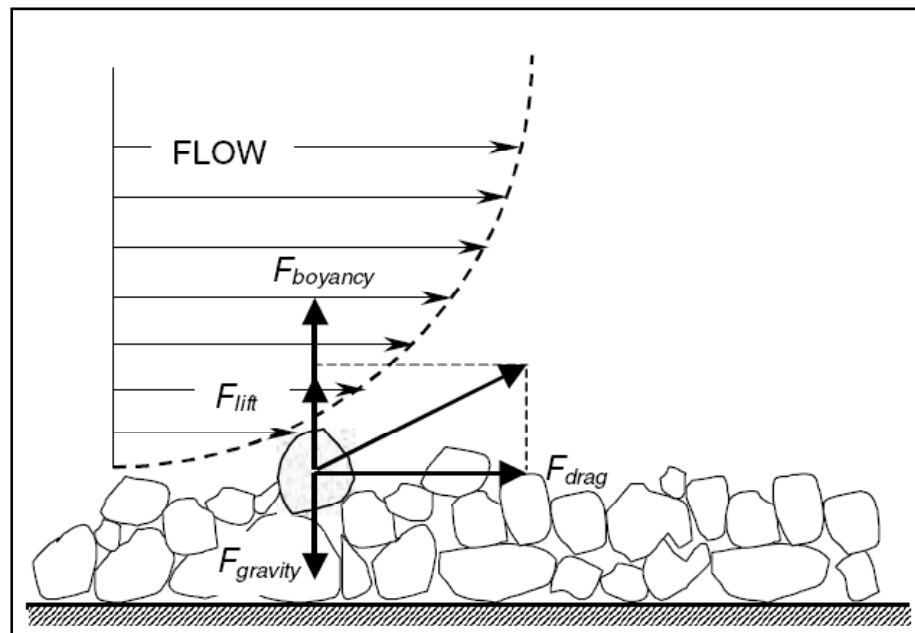


Fig 3.10- Gravitation and fluid-flow forces acting on a particle near the bottom of a horizontal pipe (stein and Hoffman, 2004)

The above equation is implicit in the variable V_s ; it must be solved by a trial-and-error technique to obtain a rigorous solution. The following, explicit equation

$$V_s = \left(\frac{1}{\beta} - \frac{\alpha}{\beta^{1.4}} \right)^{0.4} \dots\dots\dots(3.4)$$

normally provides excellent approximate answers (typically within 1% of the rigorous solution) provided,

$$\frac{\alpha}{\beta^{1.4}} < 1 \dots\dots\dots(3.5)$$

In many applications of interest, the $\alpha/\beta^{1.4}$ term is small compared to the $1/\beta$ term. This results in further simplification of Eq 1 yielding,

$$V_s = \frac{1}{\beta^{0.4}} \dots\dots\dots(3.6)$$

3.2.3 Application of Swirlers to Reduce Erosion

Swirlers are often used in oil production as a downhole desander device. They avoid sand to reach the pumping system and other pipeline accessories which results in reduced well work over and servicing activities. These separation devices are best suited for continuous flow rather than slug flow. The application of Swirlers alters the flow pattern considerably and can avoid accumulation of particles at bends and also they can

help disperse the sand particles more evenly in the flow and reduce area concentrated erosion (figure 3.11).

Pipes that encourage swirl flow can get particles into suspension at lower pumping power and lower pressure drop than a conventional round duct. Recent work (Jones, 1997; Raylor, 1998) has shown the advantages of using helically-formed pipes to induce swirl in particle-laden fluids. Helically-formed pipes of the type depicted in Fig. 3.12 were developed by Spanner (1940 and 1945) for application in low-pressure water-tube boilers.

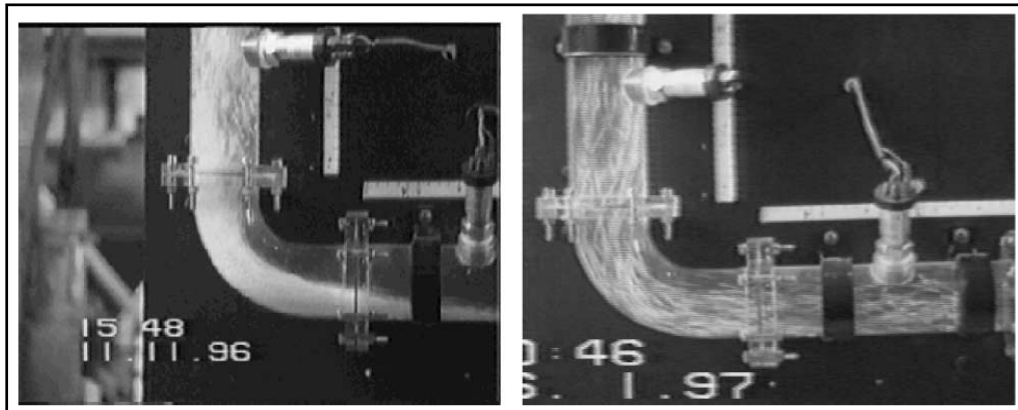


Fig 3.11 - Flow before and after introduction of swirler

(Wood, Jones, Miles, Ganeshalingam)

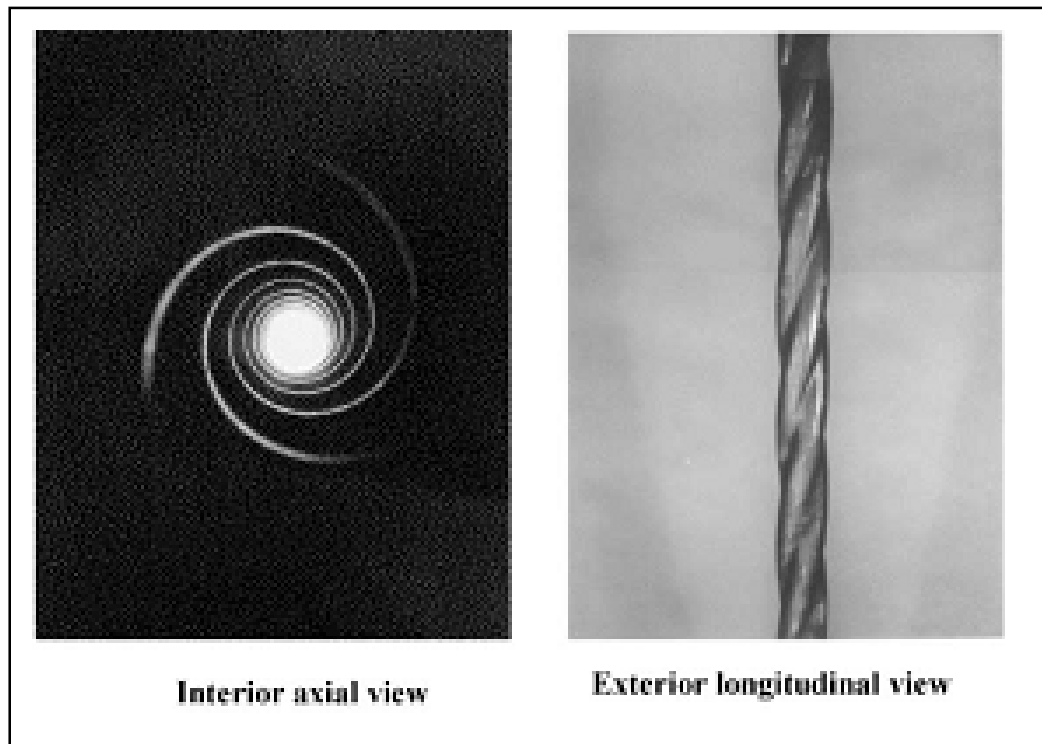


Fig 3.12 - Swirl flow boiler tube used in swirl generation

(Wood, Jones, Miles, Ganeshalingam)

3.3 Wet Gas Metering

3.3.1 Definition of Wet Gas

To date, several definitions of wet gas have been proposed within the Oil and Gas industry. All of them are equally important in covering the full range of possible stream compositions, operating pressures and temperatures, and flow regimes. Accordingly to the definition given in the SPE monograph volume 207 and as illustrated in figure 3.1, a reservoir fluid is classified as

- a) Dry gas when the reservoir temperature is greater than the criconderthem and surface/transport conditions are outside the two-phase envelope
- b) As wet gas when the reservoir temperature is greater than the criconderthem but the surface conditions are in the two-phase region
- c) As gas condensate when the reservoir temperature is less than the criconderthem and greater than the critical temperature
- d) And as an oil (volatile or black oil) when the reservoir temperature is less than the mixture critical temperature

A general definition of wet gas is a stream with liquid volume fractions between 5 and 10% at metering conditions. Following this definition, wet gas metering can be seen as the upper boundary of multiphase flow metering (oils with high gas volume fractions) and the lower boundary of gas metering (gases with high liquid volume fractions). In theory solutions to wet gas metering could, be found by pushing either multiphase flow metering or gas metering to their extremes. Due to the complexity and peculiarity of wet gas flows, wet gas metering requires a dedicated effort.

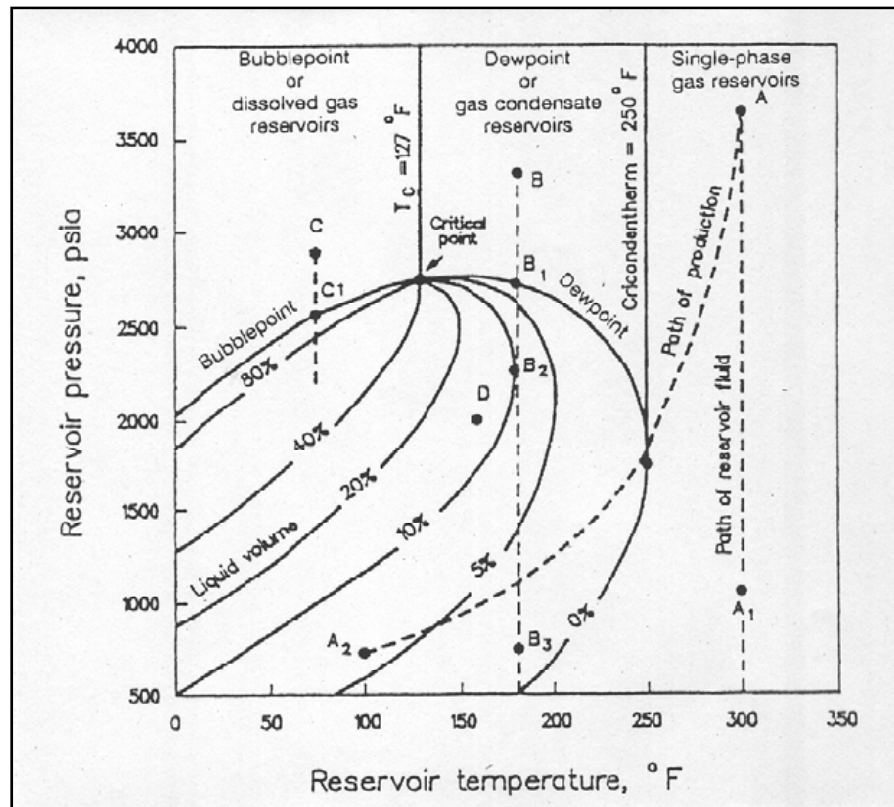


Fig 3.13 - Classification of reservoir fluids (Whitson and Brule, 2000)

3.3.2 Problems Associated with Wet Gas Metering

The problems associated with wet gas metering are

1. Slip between the liquid and the gas.
2. Difficulties in predicting the transition between flow regimes
3. Uncertainties related to the PVT characterization.
4. wet gas streams may be a combination of hydrocarbons and water, in which case wet gas metering becomes a problem in three-phases

5. Solids may also be present in the stream, so that the problem of wet gas metering extends to four phases.

Depending on the specific requirement, different metering accuracies may be required and thus different wet gas metering solutions are required. In order to account for the joint effects of flow regime, operating pressure and temperature, and liquid content of the gas, a revised classification for wet gas, based on the Lochart-Martinelli parameter (The Lockhart-Martinelli parameter is given as the square root of the ratio of the pressure gradients for the liquid and for the gas phases flowing alone in the pipe) has been recently presented. From the above brief description of wet gas, it is possible to infer that a unique metering solution for all gas condensate, high GOR and wet gas fields, based on the technologies available to date and able to satisfy every requirement in the wish list of operators, may not exist. Some wet gas meters have already been developed and made commercially available, but the majority of them are still under a testing and validation phase, both in flow loops and in the field.

3.3.3 ANUMET

An example of wet gas metering solutions is given by the ANUMET meter, described in a previous SPE paper by Falcone et al. (2003). The concept behind the ANUMET meter is that of deducing the liquid flow rate from measurements on annular flow in a straight pipe section and then using this liquid flow rate in the interpretation of pressure drop

data from a venturi placed downstream of the straight pipe section in order to deduce the gas flow rate.

The measurements are made in vertical upwards flow and are specifically for annular flow, the dominant regime involved. In sequence, the steps are as follows:

1. The annular flow flows up a tube and through a twisted tape device (with “fish tails” at its upper end),
2. Downstream of the twisted tape device, nearly all the liquid phase has been separated into the annular film on the tube wall. It continues to flow as an annular film in a straight pipe section downstream of the swirl device. Although re-entrainment of the droplets will occur, this process is relatively slow and there is an opportunity of making measurements in this region immediately downstream of the swirler in order to determine the liquid flow rate in the film and hence the total liquid flow rate if all the liquid has been separated.
3. Following the straight pipe section in which the film liquid flow rate is evaluated, the next step is to re-entrain all of the droplets into the gas stream before passing this stream into a venturi. This is done using a simple expansion contraction system that homogenizes the gas and the liquid mixture.

4. The final stage is to pass the homogenized flow through a venturi, where relationships for two-phase pressure drop calculations are used to determine the gas flow rate, knowing the liquid flow rate from step 2.

The ANUMET meter is sketched in Figure 3.14. Pinheiro (2000) carried out measurements which confirmed that good separation (efficiency higher than 90%) was possible using the twisted-tape device implemented in ANUMET, though the separation was less favorable at higher gas velocities, as illustrated in Fig.3.15.

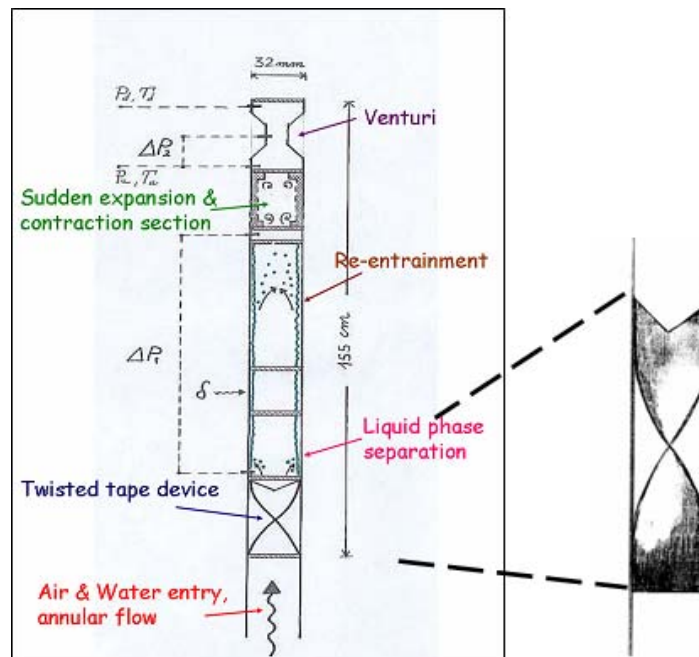


Fig 3.14 - The ANUMET wet gas metering concept

(Falcone, 2003)

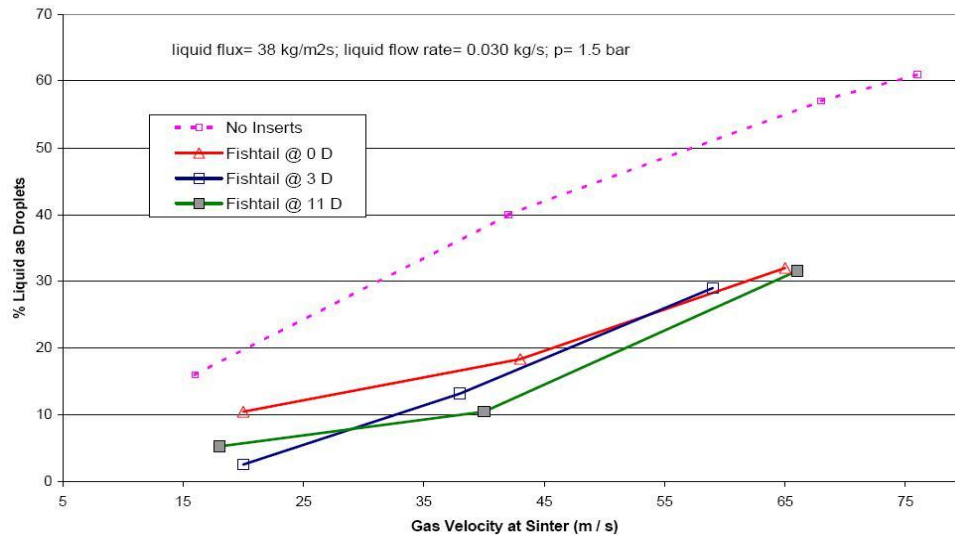


Fig.3.15 - Droplet separation efficiency at 0, 3 and 11 diameters downstream of a fish-tail twisted tape device (Pineiro, 2000)

The ANUMET metering concept introduced a novel approach to wet gas metering. In fact, although the individual devices used in ANUMET and the basic equations applied for annular flow and for homogeneous flow have been known to the Oil & Gas community for some decades now, the novelty lies in the way they have been combined towards a wet gas metering solution. The limitations of the ANUMET concept mainly relate to the instrumentation chosen for the measurements and in particular to the method used for film thickness measurement, namely gamma densitometry. Nevertheless, encouraging results have been obtained which lead to the conclusion that the system has good potential for development leading to an adequate solution to this difficult measurement problem.

CHAPTER IV

COMPUTATIONAL FLUID DYNAMICS (CFD)

In this chapter are discussed the basic concepts of CFD and the models available within the commercial software (CFX 10.0) used in this project. The main reason we are using CFD for this study is the scale and geometry we encounter in the oil and gas industry would need dedicated test facilities such as the SINTEF or NEL flow loops (Falcone, Teodoriu, Reinicke ,Bello, SPE-110116). The parameters we are interested such as liquid holdup or erosion rate, would either need very sophisticated equipment or would take a long timeline to measure. For example in the erosion studies it would take an appreciably long time to actually see the pipe material erode at the bends. CFD proves to be invaluable in this regard. Moreover since we are investigating flows which are either 2 or 3 phase flows the complexity of the problem is increased due to the interaction of these individual phases. Using CFD we can simulate flow patterns in any geometry without actually constructing it in reality. Since CFD is a simulation process there is always a deviation from reality. The output from CFD simulations are dependent on the inputs(models or boundary conditions) chosen by the individual performing these simulations. It is advisable to compare results obtained from simulations with lab/field data if available.

CFD provides excellent visualization capabilities which allows us to compare pressure or velocities along planes much more easily than conventional methods like tomography

techniques . This feature allows us to see how the variable changes over the entire span of the equipment (from inlet to outlet). CFD can simulate 2-phase flows like liquid-liquid, liquid-gas, liquid-solid, gas-solid flows and 3-phase flows like liquid-gas –solid. Using CFD also allows use to compare properties of individual phases , for example in two phase flow (air and water) we can individually compare the air and water velocity. Thus using CFD is a very effective and cheaper alternative to actual experimental studies.

4.1 Introduction

CFD is the analysis of the system involving fluids flow, heat transfer and associated phenomena such as chemical reactions by means of computer simulations. During the 1960s the aerospace industry integrated CFD techniques into the design and R&D and manufacture of aircraft and jet engines. More recently the methods have been applied to the design of internal combustion engines, combustion chamber of gas turbines and furnaces. Furthermore, automotive manufactures now routinely predict drag forces, under-bonnet air flows and the in-car environment with CFD (Versteeg and Malalasekara) .

The main aim of using CFD is to understand the physical interactions that occur in the flow of fluids around and within objects. These interactions are results of phenomena such as conduction, convection, radiation, dissipation, diffusion, shock waves, boundary

layers, and turbulence. All these phenomena are governed by the Navier-Stokes equations for compressible flow and most of these relations are nonlinear and cannot be solved analytically so numerical methods are used to solve them.

The use of numerical methods to solve partial differential equations introduces an approximation that changes the form of the basic partial differential equations. The new equations which are now obtained by changing the form of the basic partial differential equation and which are being solved by the numerical process, are referred to as the modified partial differential equations.

Since they are not the same as the original equations they will simulate the physical phenomena which is not the same as an exact solution to the basic partial differential equation would. Mathematically, these differences are usually referred to as truncation errors.

The following flowchart gives a brief overview of CFD.

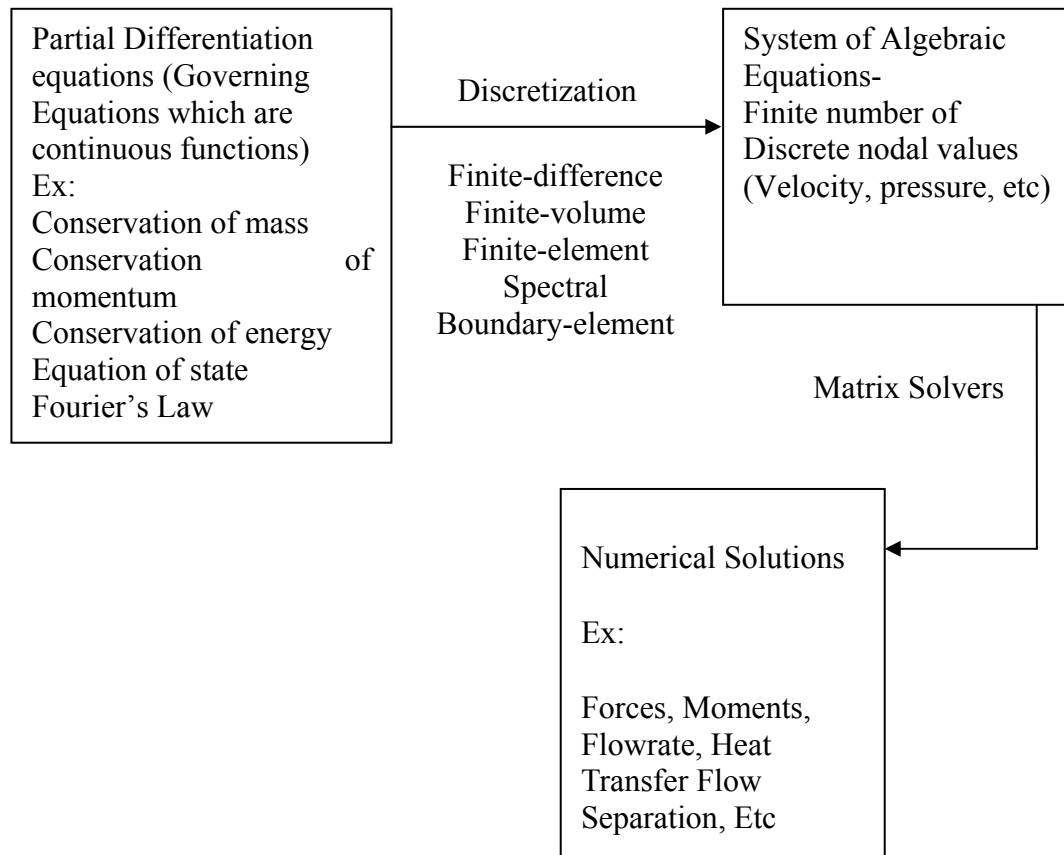


Fig 4.1 – Flowchart depicting methodology adopted in a CFD process

The procedure to correctly set up a CFD simulation is as follows:

a) Problem Specification and Geometry Preparation

The first step involves the specification of the problem, including the geometry, flow conditions and the requirements of the simulation. The geometry may result from

measurements of an existing configuration or may be associated with a design study. Flow conditions include Reynolds number, inlet velocities, mass flow rates, etc. The other requirements such as the level of accuracy needed, the turnaround time required, and the solution parameters of interest are user dependent. The first two of these requirements are often in conflict and compromise is necessary. Figure 4.2 shows a generic geometrical model built in commercially available software (ANSYS CFX 10.0).

b) Selection of Governing Equations and Boundary Conditions

Once the problem has been specified, an appropriate set of governing equations and boundary conditions must be selected. It is generally accepted that the continuum fluid flow is governed by the conservation of mass, momentum, and energy. The partial differential equations resulting from these conservation laws are referred to as the Navier-Stokes equations. Possible simplified governing equations include the potential-flow equations, the Euler equations, and the thin-layer Navier-Stokes equations.

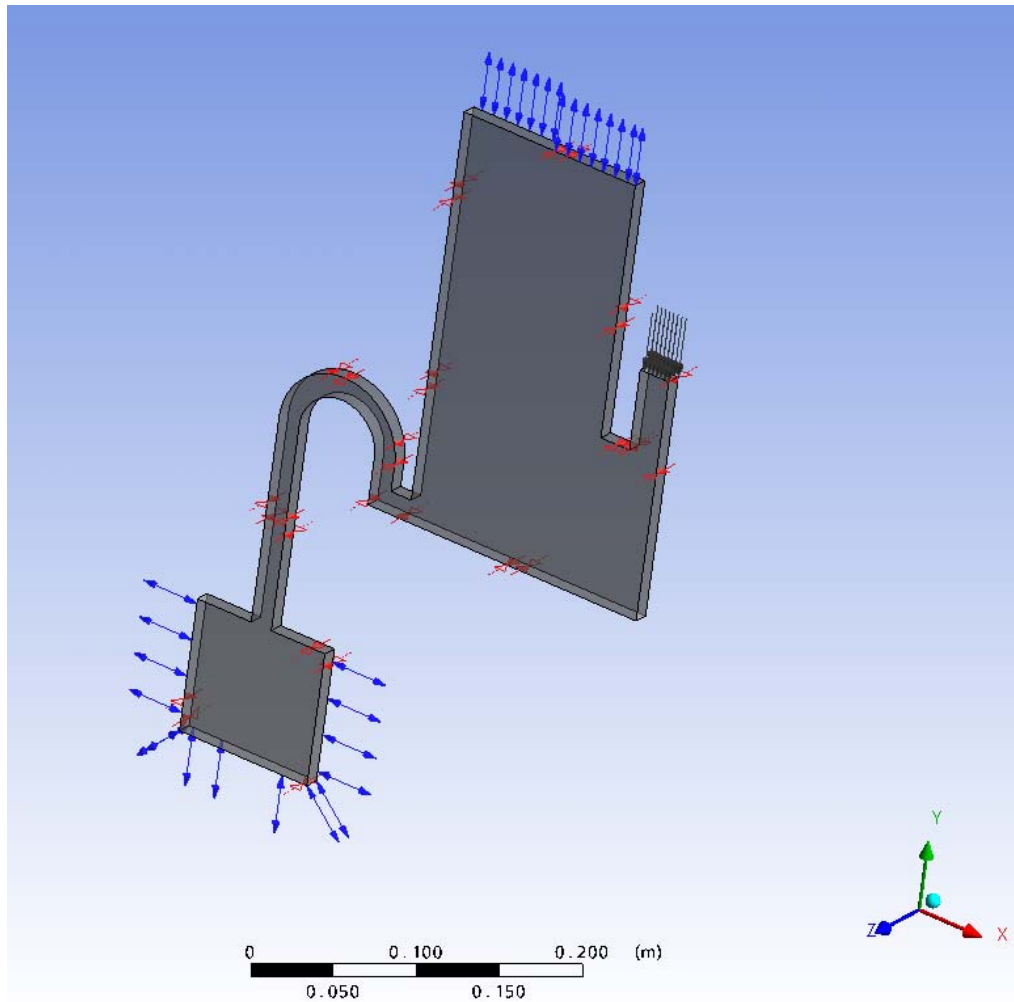


Fig 4.2 - Geometric model of a tank

These may be steady or unsteady and compressible or incompressible. Boundary types which may be encountered include solid walls, inflow and outflow boundaries, periodic boundaries, symmetry boundaries, etc. figure 4.3 illustrates these boundaries for the geometry shown in figure 4.2. The boundary conditions which must be specified depend upon the governing equations. For example, at a solid wall, the Euler equations require flow tangency to be enforced, while the Navier-Stokes equations require the no-slip

condition. If necessary, physical models must be chosen for processes which cannot be simulated within the specified constraints. The success of a simulation depends greatly on the engineering insight involved in selecting the governing equations and physical models based on the problem specification.

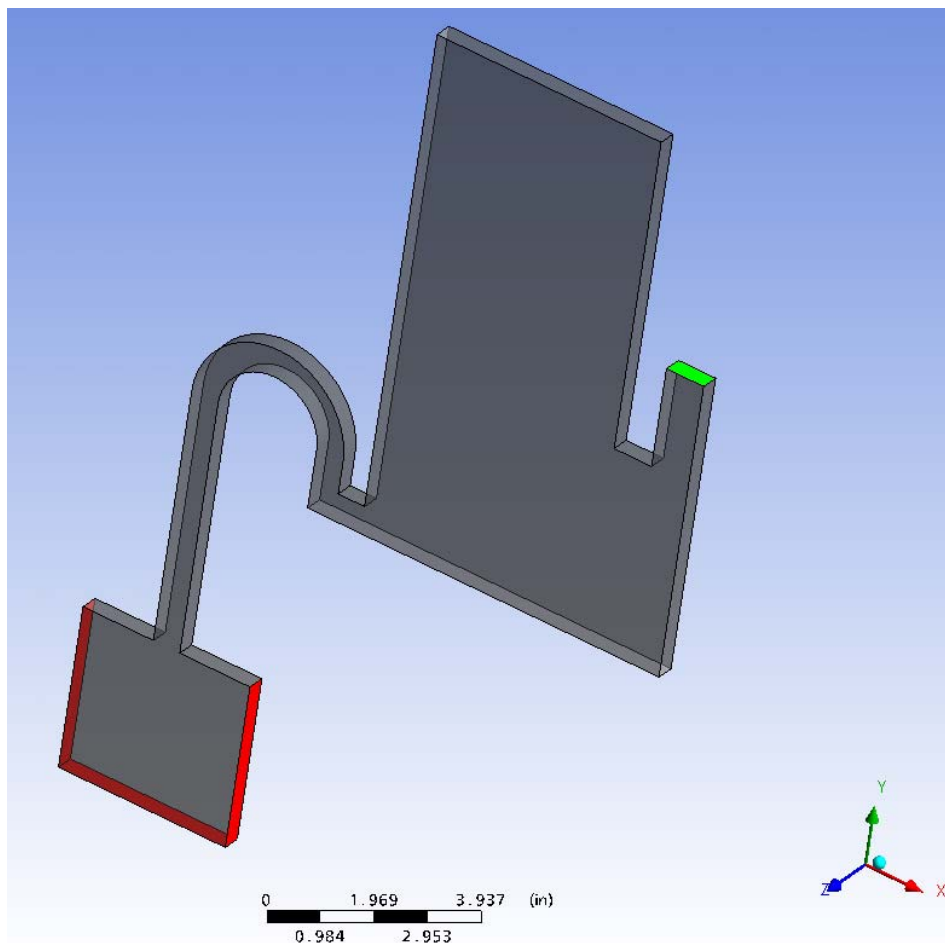


Fig 4.3 - Boundary conditions for the tank.

Inlet (Green), Outlet (Red)

c) Selection of Gridding Strategy and Numerical Method

Next a numerical method and a strategy for dividing the flow domain into cells, or elements, must be selected. Many different gridding strategies exist, including structured, unstructured, hybrid, composite, and overlapping grids. Furthermore, the grid can be altered based on the solution in an approach known as solution-adaptive gridding. Figure 4.4 shows the grid for the geometry shown in figure 4.2. The numerical methods generally used in CFD can be classified as finite-difference, finite-volume, finite-element, or spectral methods. The choices of a numerical method and a gridding strategy are strongly interdependent. For example, the use of finite-difference methods is typically restricted to structured grids. The success of a simulation can depend on appropriate choices for the problem or class of problems of interest.

d) Assessment and Interpretation of Results

Finally, the results of the simulation must be assessed and interpreted. This step can require post-processing of the data, for example calculation of forces and moments, and can be aided by sophisticated flow visualization tools and error estimation techniques. It is critical that the magnitude of both numerical and physical-model errors be well understood. Figure 4.5 shows the velocity contour for the simulation carried out on the model described in the previous figures.

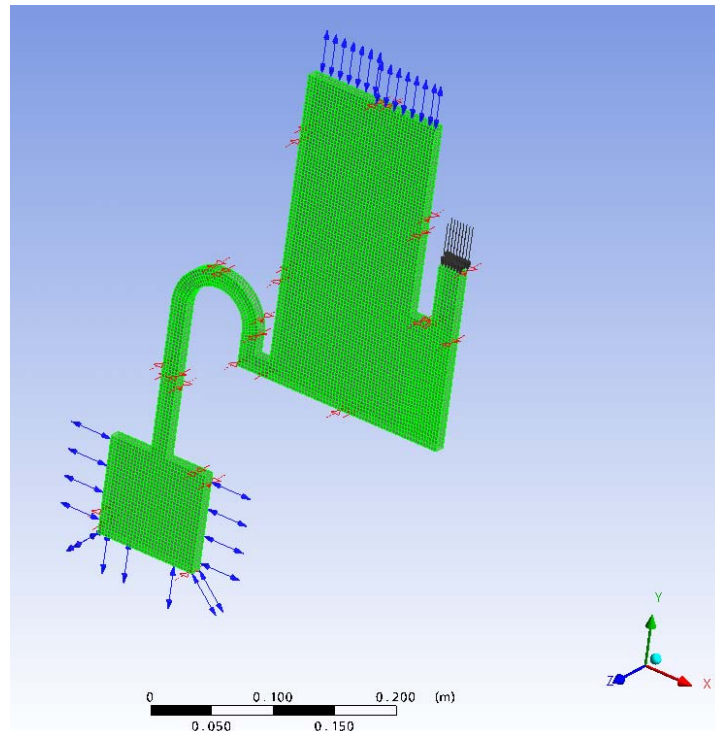


Fig 4.4 - Numerical grid for the tank model

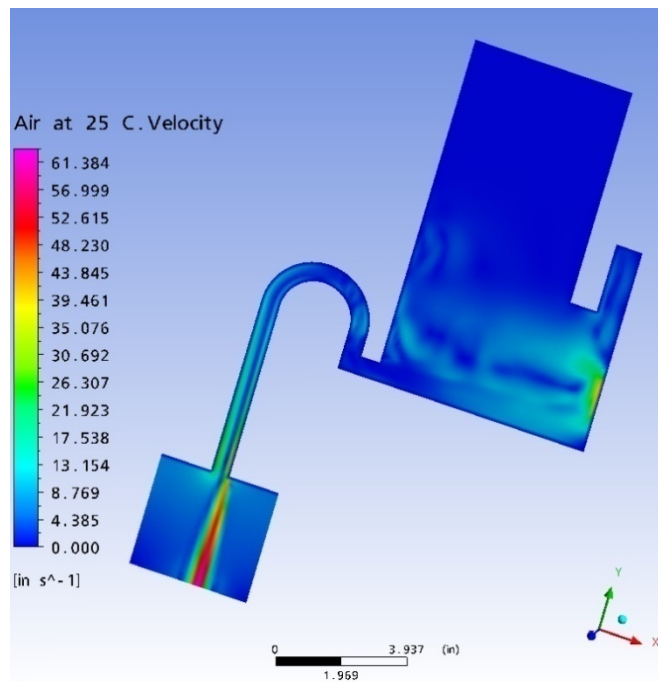


Fig 4.5 - Plot showing air velocity distribution in the tank.

4.2. Flow Modeling Techniques

There are two ways to describe the flow field, Lagrangian and Eulerian descriptions. Each of these is discussed in the following paragraphs.

4.2.1. Lagrangian Description

This is a particle approach or a “closed system” approach. In this method we confine our observations to a material volume or material surface. The material volume has a constant identifiable mass that moves with the flow but no mass crosses the material volume. The fluids in material volume will move distort and change size and shape, but always consists of the same fluid particles as shown in figure 4.6.

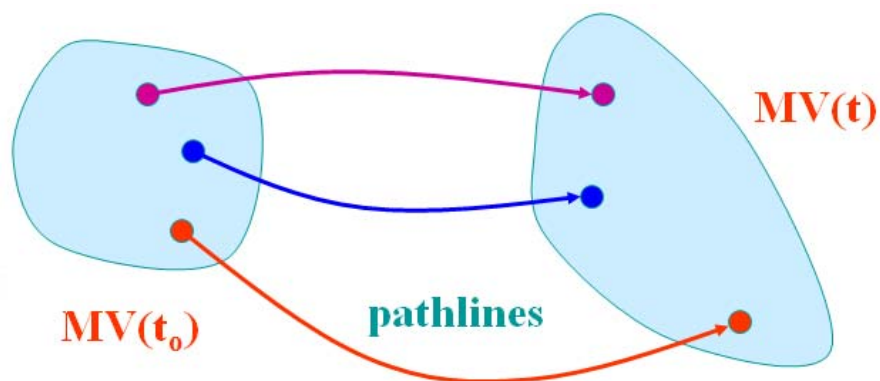


Fig 4.6 - Change in control volume

This approach is useful when we are interested in tracking particles or we are interested in particle surface interaction. This is often tedious and the time required for simulations are generally high. Figure 4.7 shows particle tracks which are a result of using this approach. The Lagrangian approach has been used in the sand erosion module of this work. By using this method we can identify the areas of the pipe where there is maximum impact and hence most erosion.

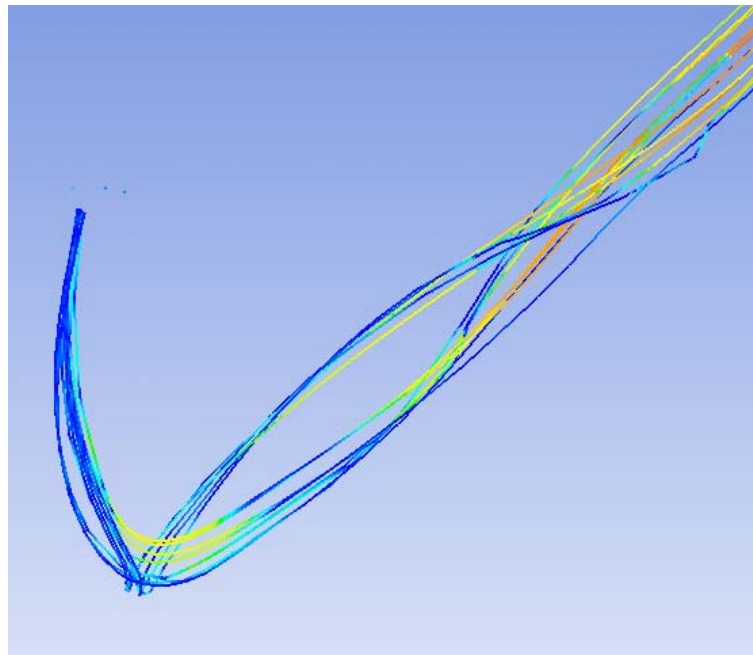


Fig 4.7 - Particle tracks of sand particles in a pipe bend obtained from CFD simulation which incorporated the Lagrangian approach

4.2.2 Eulerian Description

In this approach we analyze an “open system” where mass, momentum and energy changes occur in the control volume over time. This can be called a field approach. Individual particles are not labeled and not distinguished from one another. We focus attention on what happens at a fixed point or volume as different particles go by (figure 4.8).

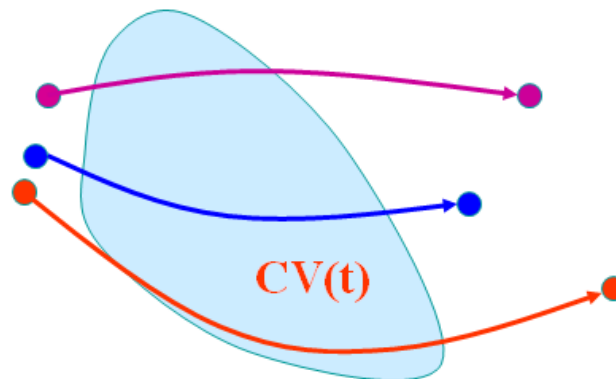


Fig 4.8 - Eulerian approach

The fixed or moving control volume may be a large system or device with inlet and outlet parts. It can also be small finite volumes generated by a computational mesh. In general, the eulerian observer is fixed to an inertial reference frame and records temporal and spatial changes of the flow field at all points inside the control volume and fluxes across its control surfaces. In contrast the Lagrangian observer stays with each fluid element or material volume and records its basic changes while moving through space.

The equations though have to be still derived from the Lagrangian approach. A surface-to-volume integral transformation then yields the conservation laws in differential form in the eulerian framework.

4.3 Governing Equations

This section briefly discusses the governing equations of flow. These equations are discretized using various techniques to break them up into algebraic equations so that they can be solved using matrix solvers.

Continuity Equation:

The continuity equation for compressible flow written in Cartesian coordinates is

$$\frac{\partial \rho}{\partial t} + \nabla \cdot (\rho \mathbf{U}) = 0 \dots\dots\dots(4.1)$$

Momentum Equations :

Momentum (M) can be written as

$$\vec{M} = \int (\rho \vec{V}) d\Omega = \int \vec{V} \rho d\Omega \dots\dots\dots(4.2)$$

Then the Lagrangian description would be

$$\frac{D}{Dt} \int \vec{V} \rho \, d\Omega = \sum \vec{F}_s + \sum \vec{F}_b \dots\dots\dots(4.3)$$

The left hand side of the equation would be rate of change of momentum of the control mass. The right hand side is the sum of all forces acting on the control mass. F_s and F_b are the surface and body forces respectively. The eulerian description of the same can be obtained by using the Reynolds transport theorem and converting the above equation to

$$\frac{d}{dt} \int \vec{V} \rho \, d\Omega + \int \vec{V} \rho \vec{V} \cdot \vec{n} \, ds = \int \rho \vec{f} \, d\Omega + \int \vec{T} \cdot \vec{n} \, ds \dots\dots\dots(4.4)$$

Navier-Stokes Equations:

The Navier–Stokes equations describe the motion of a viscous fluid. These equations are obtained by applying Newton's second law to fluid motion, coupled with which is the sum of a diffusing viscous term which is proportional to the gradient of velocity, and a pressure term. The Navier–Stokes equations are differential equations which relate the rates of changes of the variables like velocity and pressure. For an incompressible fluid with a constant viscosity the Navier-stokes equation can be written as

$$\rho \frac{D\vec{V}}{Dt} = \rho \vec{f} - \nabla p + \mu \nabla^2 \vec{V} \dots\dots\dots(4.5)$$

For a compressible fluid the equations are

$$\rho \frac{D\vec{V}}{Dt} = \rho \vec{f} - \nabla p + \mu \nabla^2 \vec{V} + \frac{1}{3} \mu \nabla (\nabla \cdot \vec{V}) \dots \dots \dots (4.6)$$

It has to be noted that the equations mentioned above are generic and depending on the coordinate system chosen vary accordingly. In any case there are 3 equations which collectively are referred to as the Navier-stokes Equations. In the following sections we discuss the models which were used in this work.

4.4 Homogeneous Model

In homogeneous multiphase flow, a common flow field is shared by all fluids, as well as other relevant fields such as temperature and turbulence. This allows some simplifications to be made to the multi-fluid model resulting in the homogeneous model. For a given transport process, the homogeneous model assumes that the transported quantities (with the exception of volume fraction) for that process are the same for all phases.

Since transported quantities are shared in homogeneous multiphase flow, it is sufficient so solve for the shared fields using bulk transport equations rather than solving individual phasic transport equations. The bulk transport equations can be derived by summing the individual phasic transport equations over all phases to give a single transport equation. The homogeneous model does not need to be applied consistently to

all equations. For example, the velocity field may be modeled as inhomogeneous, but coupled with a homogeneous turbulence model. Alternatively, a homogeneous velocity field may be coupled with inhomogeneous temperature fields.

4.5 Inhomogeneous Model

In the inhomogeneous model the transport equations are solved individually for each phase. This would mean twice or thrice the number of equations for a single phase flow and would be computationally more expensive. Since all the flow patterns cannot be solved using homogenous model several sub-models are available in CFX which will allow us to efficiently use the inhomogeneous model. Sections 4.5.1 ,4.5.2 and 4.5.3 describe such models available in CFX which have been used in this study.

Interfacial transfer of momentum, heat and mass is directly dependent on the contact surface area between the two phases. This is characterized by the interfacial area per unit volume between phase α and phase β , known as the interfacial area density, $A_{\alpha\beta}$. The following three sections describe the various models which model Interfacial transfer. These essentially provide different algebraic prescriptions for the interfacial area density.

4.5.1 The Particle Model

The Particle model for interfacial transfer between two phases assumes that one of the phases is continuous (phase α) and the other is dispersed (phase β). The surface area per unit volume is then calculated by assuming that phase β is present as spherical particles of Mean Diameter d_β (which has to be specified by the user). Using this model, the interphase contact area is:

$$A_{\alpha\beta} = \frac{6 r_\beta}{d_\beta} \dots\dots\dots(4.7)$$

Where r_β is the volume fraction of phase β . The other Non-dimensional interphase transfer coefficients are defined in terms of the mean diameter, and the continuous phase properties. Reynolds number is defined as

$$Re_{\alpha\beta} = \frac{\rho_\alpha}{\mu_\alpha} |U_\beta - U_\alpha| d_\beta \dots\dots\dots(4.8)$$

and the fluid Prandtl number as

$$Pr_{\alpha\beta} = \frac{\mu_\alpha}{\lambda_\alpha} C_{p\alpha} \dots\dots\dots(4.9)$$

Where U_i is the velocity magnitude, C_p is the specific heat capacity and λ is the thermal conductivity.

4.5.2 The Mixture Model

This is a very simple model which treats both phases α and β symmetrically. The surface area per unit volume is calculated from

$$A_{\alpha\beta} = \frac{r_\beta r_\alpha}{d_{\alpha\beta}} \dots\dots\dots(4.10)$$

Where $d_{\alpha\beta}$ is the interfacial length scale, which must be specified.

Reynolds number is defined as

$$Re_{\alpha\beta} = \frac{\rho_{\alpha\beta}}{U_{\alpha\beta}} |U_\beta - U_\alpha| d_{\alpha\beta} \dots\dots\dots(4.11)$$

and the fluid Prandtl number as

$$Pr_{\alpha\beta} = \frac{\mu}{\lambda_{\alpha\beta}} C_{P\alpha\beta} \dots\dots\dots(4.12)$$

Where $\rho_{\alpha\beta}$, $\mu_{\alpha\beta}$, $C_{P\alpha\beta}$ and $\lambda_{\alpha\beta}$ are the density, viscosity, specific heat capacity and thermal conductivity of the mixture defined by

$$\rho_{\alpha\beta} = r_\alpha \rho_\alpha + r_\beta \rho_\beta \dots\dots\dots(4.13)$$

$$\mu_{\alpha\beta} = r_\alpha \mu_\alpha + r_\beta \mu_\beta \dots\dots\dots(4.14)$$

Where U_i is the velocity magnitude, C_p is the specific heat capacity and λ is the thermal conductivity.

4.5.3 The Free Surface Model

The free surface model attempts to resolve the interface between the fluids. If there are just two phases in the simulation, the following equation is used for interfacial area density:

$$A_{\alpha\beta} = |\nabla r_\alpha| \dots \dots \dots (4.15)$$

if there are more than two phases then it is generalized as follows

$$A_{\alpha\beta} = \frac{2|\nabla r_\alpha| |\nabla r_\beta|}{|\nabla r_\alpha| + |\nabla r_\beta|} \dots \dots \dots (4.16)$$

4.6 Simulating Turbulence

Almost all fluid flow which we encounter in daily life is turbulent. Typical examples are flow around (as well as in) cars, airplanes and buildings. The boundary layers and the wakes around and after bluff bodies such as cars, airplanes and buildings are turbulent. Also the flow and combustion in engines, both in piston engines and gas turbines and combustors, are highly turbulent. Air movements in rooms are also turbulent, at least

along the walls where wall-jets are formed. The flow in the separator is turbulent, and this creates one problem when using CFD.

In principle, if the computational grid could be made fine enough, CFD could be used to solve the Navier-Stokes equations directly, and the turbulence would automatically arise in the simulation. In 'direct turbulence modeling' such CFD simulations are already being carried out in small, simple geometries and this field is advancing fast as the computational power increases. However, in real processing equipment, this is not possible yet. The number of grid points and time steps required is too high. For this reason 'turbulence models' are required.

These are meant to mimic the influence on the turbulence on the mean fluid flow pattern. Correctly mimicking the effect of the turbulence is especially difficult in swirling flows. Almost all the flows encountered in the oil and gas industry are turbulent in nature. Turbulence effects are prominent at the wall (pipe surface).

There is no definition on turbulent flow, but it has a number of characteristic features (Tennekes & Lumley) such as:

- a) Irregularity- Turbulent flow is irregular, random and chaotic. The flow consists of a spectrum of different scales where largest eddies are of the order of the flow geometry (i.e. boundary layer thickness, jet width, etc). At the other end of there are

smallest eddies which are by viscous forces dissipated into internal energy. Even though turbulence is chaotic it is deterministic and is described by the Navier-Stokes equations.

- b) Diffusivity- In turbulent flow the diffusivity increases. This means that the spreading rate of boundary layers, jets, etc. increases as the flow becomes turbulent. The turbulence increases the exchange of momentum in e.g. boundary layers and reduces or delays thereby separation at bluff bodies such as cylinders, airfoils and cars. The increased diffusivity also increases the resistance (wall friction) in internal flows such as in channels and pipes.
- c) Large Reynolds Numbers- Turbulent flow occurs at high Reynolds number. For example, the transition to turbulent flow in pipes occurs around $Re = 2000$ and in boundary layers around $Re = 100000$.
- d) Three Dimensional - Turbulent flow is always three-dimensional. However, when the equations are time averaged we can treat the flow as two-dimensional.
- e) Dissipation - Turbulent flow is dissipative, which means that kinetic energy in the small (dissipative) eddies are transformed into internal energy. The small eddies receive the kinetic energy from slightly larger eddies. The slightly larger eddies receive their energy from even larger eddies and so on. The largest eddies extract

their energy from the mean flow. This process of transferred energy from the largest turbulent scales (eddies) to the smallest is called cascade process.

- f) Continuum - Even though we have small turbulent scales in the flow they are much larger than the molecular scale and we can treat the flow as a continuum.

The velocity components in the Navier-Stokes equations are split in two parts:

- a) a fluctuating part due to the turbulence with a mean of zero and
- b) a mean part,

The equations are then time-averaged; the effect of the turbulence appears as extra stresses augmenting those caused by the molecular viscosity. These extra stresses are called the 'Reynolds stresses'. There are 9 Reynolds stresses, 3 in each of the three coordinate planes. It can be shown that the Reynolds stress tensor is symmetrical, so that only 6 of the stresses are independent. Reynolds stresses again give rise to the notion of a 'turbulent viscosity' augmenting the molecular one.

In most practical situations, the turbulent viscosity turns out to be much higher than the molecular one. Contrary to the molecular viscosity, the turbulent viscosity needs neither to be homogeneous, i.e. the same at all points in the flow field, nor isotropic, i.e. the same in all directions.

The standard k - ϵ model is used in the prediction of most turbulent flow calculations because of economy and reasonable accuracy for a wide range of flows. In the ‘ k - ϵ turbulence model’, equations are solved for the turbulence kinetic energy per unit mass, k , and the dissipation rate of the turbulence per unit mass, ϵ . However, the model does not work well when it encounters with non-equilibrium boundary layers.

It predicts the onset of separation very late and also underpredicts the degree of separation. Separation defines the performance of many devices, such as turbine blades, aerodynamic bodies and diffusers. Separation also influences wall heat transfer and multi-phase phenomena. Predicting reduced separation results in an optimistic prediction of machine performance. In some applications, this may have dangerous consequences, for example - the prediction of wing stall on airplanes.

In the ‘Reynolds stress model’, or ‘RSM’, transport equations are solved for all 6 independent Reynolds stresses. These transport equations are formulated by modifying the time-averaged Navier-Stokes equations, but it is very tedious to solve all these coupled equations. In the ‘algebraic stress model’ or ‘ASM’, the transport equations for the Reynolds stresses are rewritten as algebraic expressions by assuming that the ‘transport of the stresses’ around the flow field is proportional to the transport of the turbulent kinetic energy, k .

The ASM gives conceptual problems in swirling flows, and for this reason Boysan et al. (1986) formulated a hybrid between ASM and RSM in which transport equations for some stress components are solved, while, for the rest, the algebraic expressions from the ASM are used. The newest technique is ‘Large Eddy Simulation’ or LES, where the larger eddies, which are mostly responsible for anisotropy in the turbulence, are simulated directly, while the effect of the smaller eddies is accounted for in a simple turbulence model.

To solve this problem, better models are available. One of the most effective is the shear stress transport (SST) model of Menter. The model works by solving a turbulence/frequency-based model ($k-\omega$) at the wall and $k-\epsilon$ in the bulk flow. A blending function ensures a smooth transition between the two models.

4.7 Erosion Model

The wear of a wall due to the erosive effect of particle impacts is a complex function of particle impact, particle and wall properties. For nearly all metals, erosion is found to vary with impact angle and velocity according to the relationship given below (equation 4.17).

$$E = K V_p^n f(\gamma) \dots \dots \dots (4.17)$$

Where E is a dimensionless mass, V_p is the particle impact velocity and $f(\gamma)$ is a dimensionless function of the impact angle. The impact angle is the angle in radians

between the approaching particle track and the wall. The value of the exponent, n , is generally in the range 2.3 to 2.5 for metals. Finnie's model (available in CFX10.0) of erosive wear relates the rate of wear to the rate of kinetic energy of impact of particles on the surface, using $n=2$. So equation 4.17 changes to

$$E=K V_p^2 f(\gamma) \dots \dots \dots (4.18)$$

where

$$f(\gamma) = \frac{1}{3} \cos^2(\gamma) \quad \text{if } \tan(\gamma) > 1/3$$

$$f(\gamma) = \frac{1}{3} \cos^2(\gamma) \quad \text{if } \tan(\gamma) > 1/3 \dots \dots \dots (4.19)$$

4.8 Other Applications of CFD

The technique is very powerful and spans a wide range of industrial and non-industrial application areas. Some examples are

- a) Aerodynamics of aircraft and vehicles: lift and drag.
- b) Hydrodynamics of ships.
- c) Power plant: combustion of IC engines and gas turbines.
- d) Turbomachinery: flow inside rotating passages and diffusers etc.

- e) Electrical and electronic engineering: cooling of equipments including micro-circuits.
- f) Chemical process engineering: mixing and separation, polymer moulding.
- g) External and internal environment of buildings, wind loading and heating/ventilation, Marine engineering: loads on offshore structures.
- h) Environmental engineering: distribution of pollutants and effluents.
- i) Hydrology and oceanography: flows in rivers, estuaries, oceans.
- j) Biomedical engineering: blood flows through arteries and veins.

CHAPTER V

NUMERICAL INVESTIGATION OF SWIRL FLOWS

The approach adopted is to first simulate experimental flow patterns for which entire data is available. This helps us understand how well/accurately CFD reproduces the flow. This also helps us to pick the correct flow and turbulence models. If we are able to match the experimental results within an acceptable range then we can confidently simulate proposed flows and accept the results. Simulating swirl flows like those in ANUMET helps us better understand the physics of two phase or multiphase flow which are vital in understanding how the downhole tools for liquid loading or sand erosion control work.

5.1. ANUMET Validation

In the actual ANUMET rig the length of pipe was about 10m before it encountered the swirler. In order to achieve computational efficiency a sensitivity analysis on the length of the pipe before swirler was conducted and a length of 2.5m facilitated fully developed annular flow before the swirler. Initial results indicated that the expansion and contraction section in the actual Anumet model (figure 5.2) did not have any impact on the results. So they were excluded from the following simulations and a simplified geometry was created (figure 5.3) to decrease the mesh size and improve time taken for the simulation. Since the volume fraction of water was very low and the high magnitude

of velocity in the pipe an inflated boundary layer was used to capture the water flow accurately (figure 5.4). The total mass flow rate and the volume fractions of water and air were specified at the inlet. The outlet was left open to atmosphere (1 atm). This was to ensure that the flow was not against a pressure.

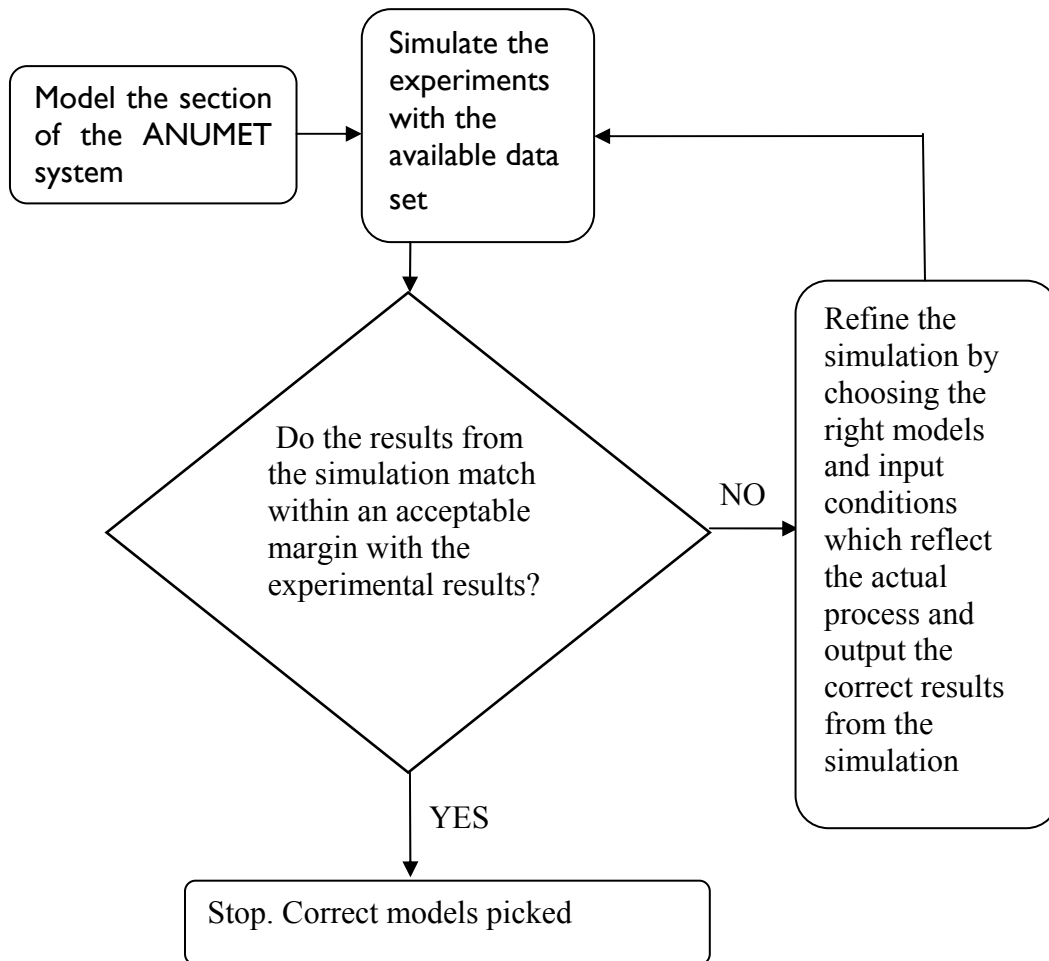


Fig 5.1- Flow chart depicting the methodology adopted for the ANUMET Validation process

The following assumptions/models were made/selected prior to running the simulations:

- a) Steady-state, subsonic flow.
- b) Scalable k- ϵ turbulence model.
- c) Fluid temperature equal to 25 °C and isothermal heat transfer process (the simulations proved insensitive to fluid temperature).
- d) Surface tension not accounted for, due to the high flow velocity involved.
- e) Drag coefficient equal to 0.44.
- f) Flow direction normal to inlet /outlet.
- g) Mass flow rates and volumetric phase fractions specified at the inlet.
- h) Outlet defined as a pressure outlet, open to the atmosphere.
- i) Convergence assumed to be achieved when the residuals obtained after solving the equations drop to 10E-4.
- j) Eulerian – Eulerian multiphase model. This is best suited for the case at hand. The other option was to use the Lagrangian multiphase model, but this is more appropriate in the case of suspended particles or particle tracking.

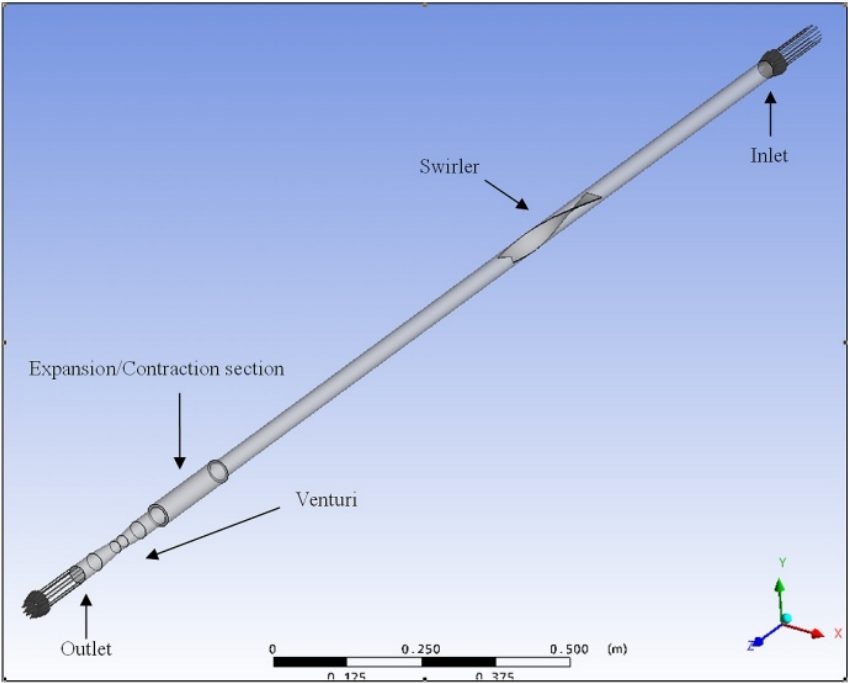


Fig 5.2- Actual ANUMET geometry as modeled with CFX before modifications

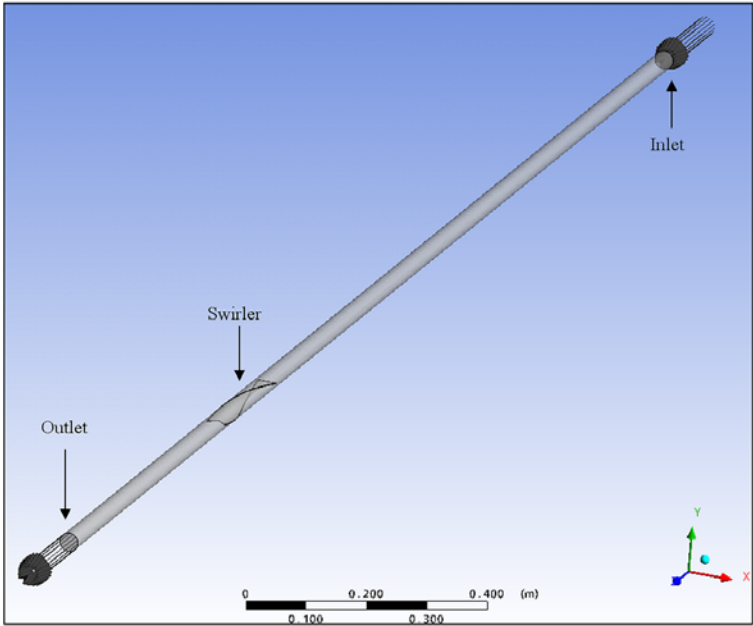


Fig 5.3- Simplified ANUMET geometry as modeled with CFX

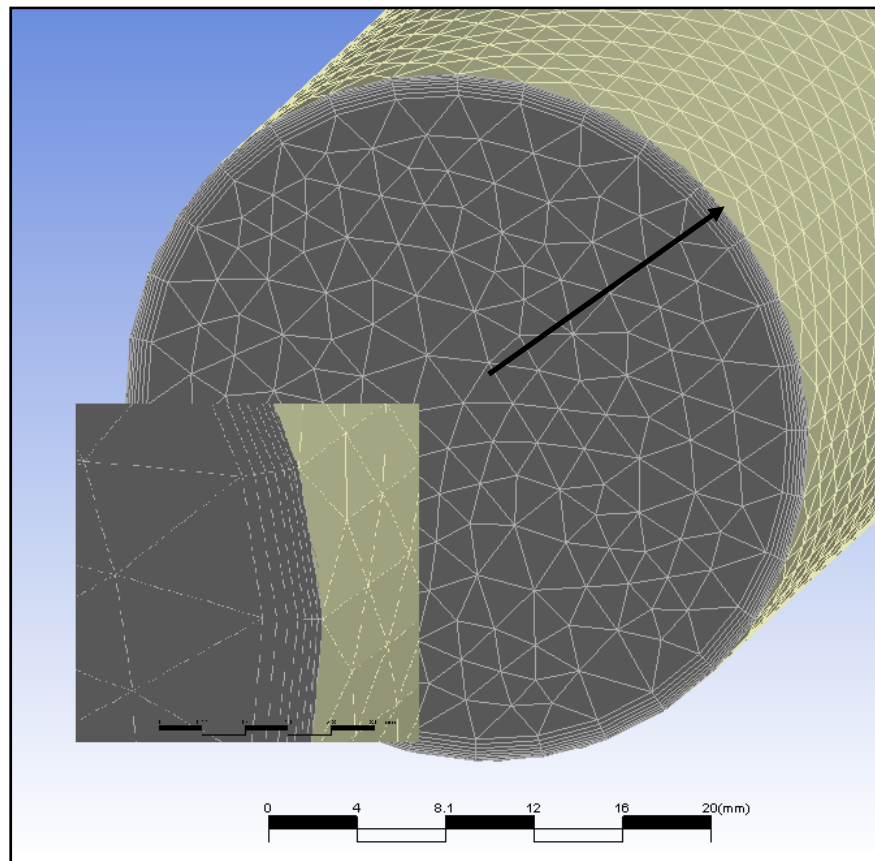


Fig 5.4 - Inflated boundary at pipe wall as modeled with CFX

5.2 Liquid Loading

For the liquid loading application - which can be seen as an upscaled version of the dimensions investigated in the wet gas metering application, the main focus was the liquid hold-up parameter. It is defined as the ratio of area occupied by liquid to the total area. In order to check if the introduction of a swirler actually helps liquid unloading we need to understand the relation between the liquid hold up and water flow rate.

In order to do this a series of simulations with a constant gas rate and a variable water rate are performed and the variation in liquid hold up is observed.

5.3 Erosion in Pipes

The effect of a swirler in reducing erosion at pipe bends was investigated in a twofold manner. The first step was to compare the erosion rate on the pipe surface without the swirler and the erosion rate after the introduction of the swirler by performing CFD simulations on a pipe bend which is subject to erosion by solid particles suspended in a liquid impinging on the inner wall or surface. The second step was to design a multiphase test loop (in room 601, 6th floor, Richardson bldg) where erosion studies can be conducted.

The length of the loop was agreed upon as 12 ft keeping in mind the available space in the room and other equipment that would be connected to the loop. Transparent Perspex pipe was decided upon as the material as it would allow us to clearly see inside the pipe and also allow the usage of PIV (Particle image velocimetry - an optical method used to measure velocities and related properties in fluids) or High speed cameras to capture images inside the pipe. The main variable was the pipe diameter. In order to pick the right pipe diameter CFD simulations were planned on 3 pipe diameters to decide which pipe diameter would suit our requirements correctly.

CHAPTER VI

RESULTS

6.1. ANUMET Validation

The following sections describe the results from the simulations done on the swirling section of the ANUMET system. In order to correctly capture the flow phenomenon picking the right model which mimics the flow pattern was necessary so some of the models were tested and the appropriate flow model was selected based on the results.

The following table tabulates the data (Falcone ,2003) used for the following simulations

Table 6.1 Parameters used in the simulation.

Water Mass flux	769.81 kg/m ² /s
Gas Mass Flux	128.31 kg/m ² /s
Total flow rate	0.726 kg/s
Water flow rate	0.622 kg/s
Gas flow rate	0.103 kg/s
Volume fraction of water	0.007
Volume fraction of Gas	0.993
Inlet Diameter of Pipe	32.1 mm

The homogenous model is a simplification from the multifluid model. The homogenous model assumes that for a given transport process, the transported quantities (with the exception of volume fraction) for that process are the same for all phases. It solves for the shared fields using bulk transport equations rather than solving individual phasic transport equations. This results in lower simulation time because of the less number of equations to be solved. But this model predicted wrong values for for this specific case. The maximum and minimum values for density were 22.098 kg/m^3 and 2.534 kg/m^3 (Figure 6.1) where as the expected values for maximum and minimum density were 997 kg/m^3 (density of water) and 1.085 kg/m^3 (density of air) respectively.

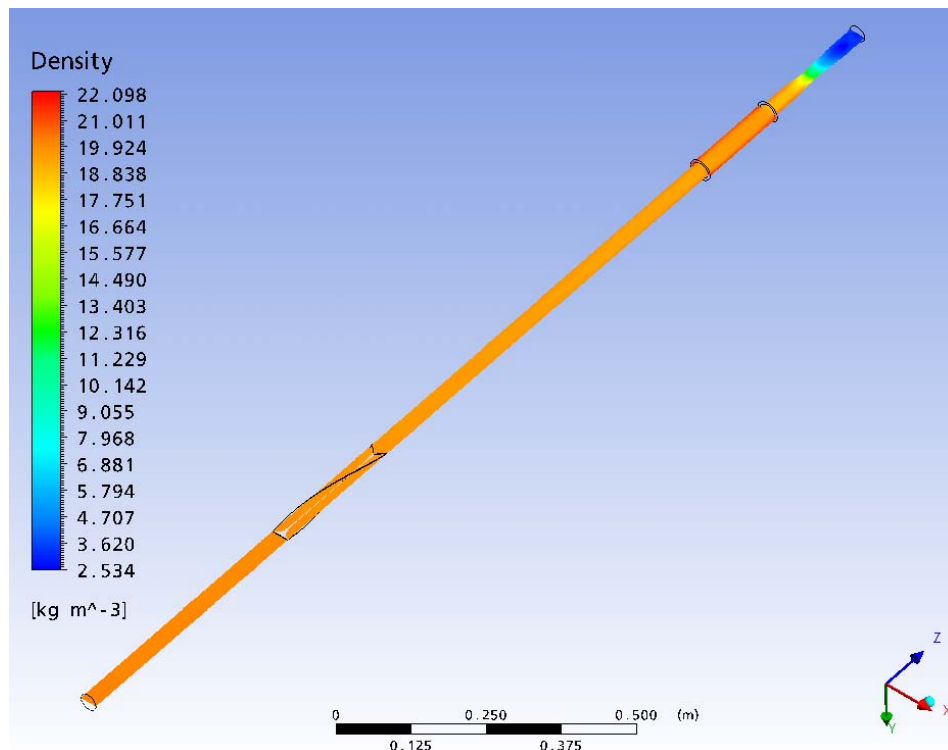


Fig 6.1 Values for density- Homogeneous model

This prediction of densities was enough to indicate that this model was not correctly replicating the flow process. Also this model did not predict the separation of phases after flow past the swirl which can be observed in figure 6.1 (Density plotted on the center plane). there is no change in the distribution of density after the flow has passed the swirler. We would expect a higher density at the pipe walls due to the centrifugal force imparted by the swirler, but that does not happen here.

The use of the inhomogeneous model proved to be an improvement over the homogenous model. In the inhomogeneous model the flow equations are solved independently for each phase. The time required for this simulation is longer (compared to the homogenous model), but the results are more realistic in this. The separation of phases and the range of densities were definitely acceptable. The fluid film which was observed in the actual experiments was also clearly observed in the results. Two kinds of sub-models were available within the inhomogeneous model. The results of each of these are discussed in the following sections.

When the mixture model was used there was an immediate improvement in the results. The range of densities was 992.06kg/m^3 and 13.84 kg/m^3 which was definitely better than 22.098 kg/m^3 and 2.534 kg/m^3 predicted by the homogenous model. Though the range is entirely not true it was closer to reality than the previous results. Figure 6.2 illustrates the ranges of density and figure 6.3 shows the fluid film reproduced by the CFD model, which was also observed in the experiments reported by Falcone(2003).

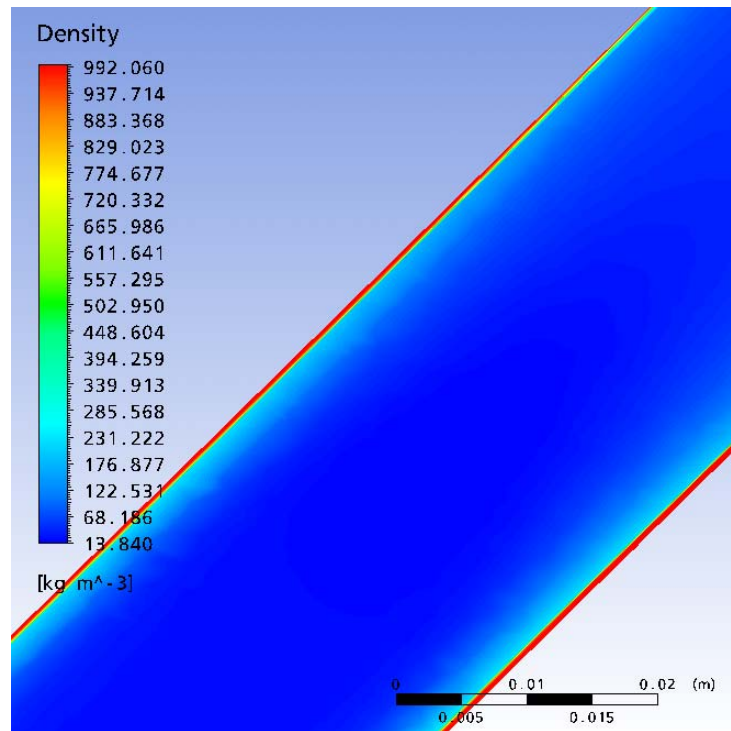


Fig 6.2 - Separation of phases. Water is concentrated along the pipe wall (red) resulting in a fluid film

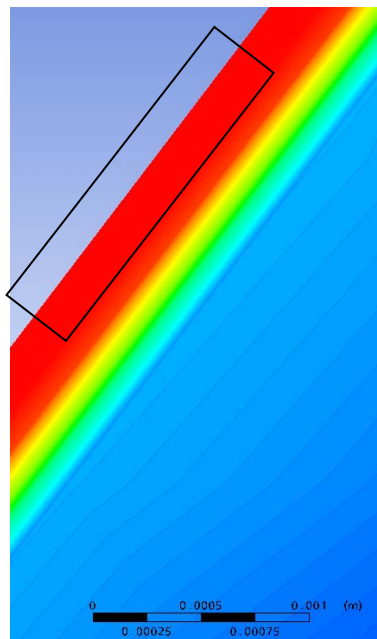


Fig 6.3 - Fluid film (Red band) at the pipe wall

When the free surface model was used the results were even better. The range of densities was 997.06kg/m^3 and 2.069 kg/m^3 (figure 6.4). This was an improvement over the density range 992.06kg/m^3 and 13.84 kg/m^3 . The upper limit corresponds to density of water and the lower limit is closer to the density of water.

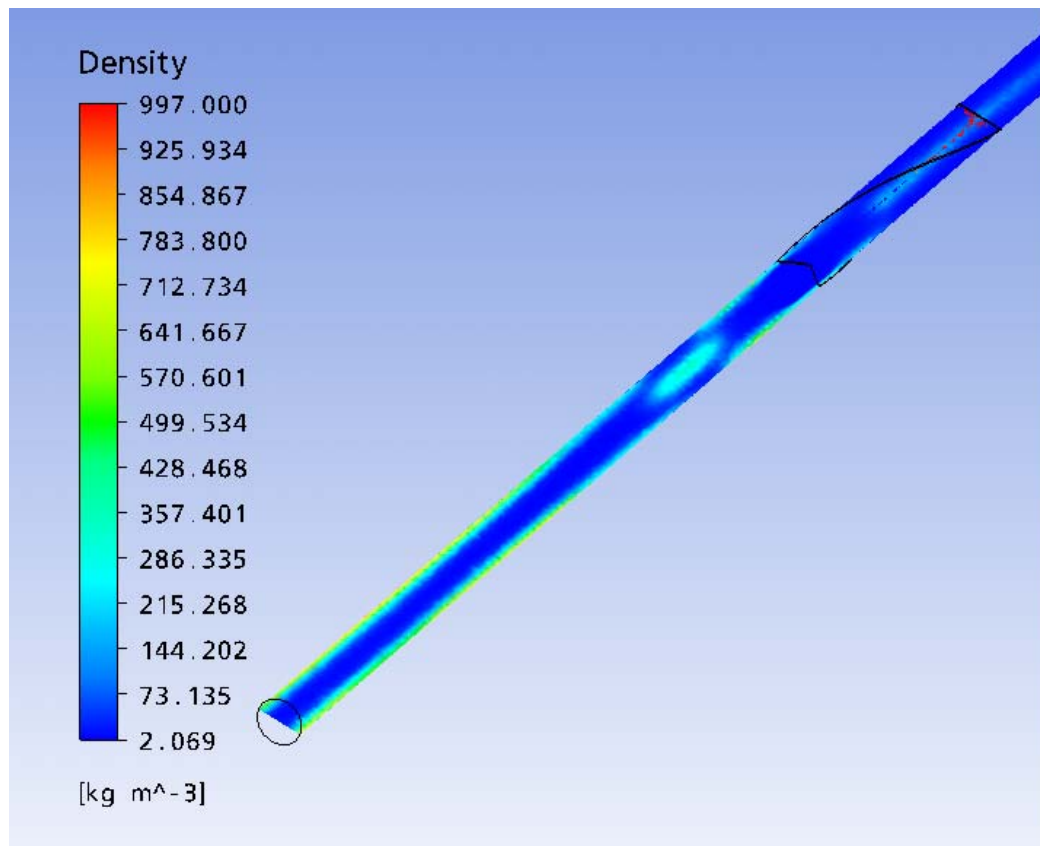


Fig 6.4 - Density ranges predicted by the free surface model

In summary, the best match of results was obtained with the inhomogeneous model, in combination with the free surface model. Compared to the corresponding experimental value, the predicted pressure drop is 1.52 psi higher. A sensitivity analysis of the

simulation model is required to investigate the reasons for this mismatch and more data points are needed to verify whether the problem persists at different input rates. The film thickness, predicted by the simulation, was 0.75mm, whereas the actual value measured during the reported experiments was 0.69mm (Falcone, 2006). This is considered to be an acceptable result, considering the accuracy of the experimental measurements of the liquid film thickness.

6.1.1. Maximum Liquid Deposition

In order to see where there is maximum liquid deposition when using the ANUMET meter a series of simulations was done. Table 2 is a summary of the input flow rates and volume fractions for water and air used in the simulations. The range of distances downstream of the swirler where there is maximum deposition is recorded from the simulations and tabulated. Figure 6.5 shows how maximum deposition is measured.

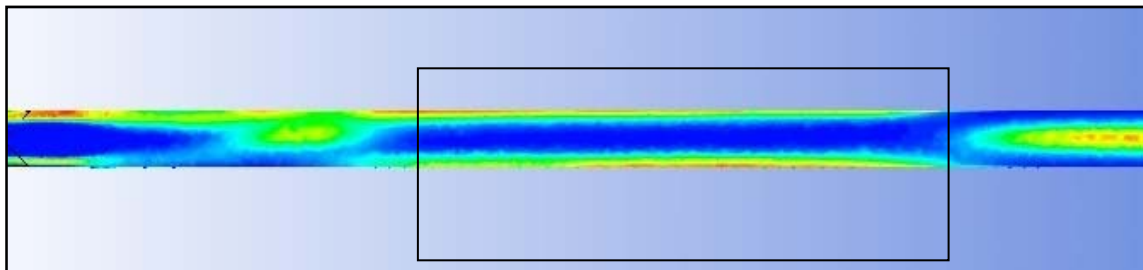


Fig 6.5 - Maximum liquid deposition

Table 6.2 Input parameters for simulations

RUN	gas flow rate (Kg/s)	water flow rate (Kg/s)	Volume fraction of water	Volume Fraction of gas	Distance Downstream of Swirler (cm)	
					Lower Limit	Upper Limit
2	0.0382	0.0834	0.0026	0.9974	26.082	49.990
3	0.0531	0.0834	0.0019	0.9981	17.390	74.000
4	0.0937	0.0834	0.0011	0.9989	8.694	28.255
5	0.1068	0.0834	0.0009	0.9991	8.694	26.082
10	0.0599	0.2220	0.0044	0.9956	34.776	75.203
11	0.0813	0.2220	0.0032	0.9968	13.041	56.511
12	0.1098	0.2220	0.0024	0.9976	10.868	43.470
13	0.1287	0.2220	0.0020	0.9980	10.868	54.338
16	0.0284	0.3644	0.0150	0.9850	21.735	30.429
17	0.0440	0.3644	0.0097	0.9903	60.858	80.420
19	0.0785	0.3644	0.0055	0.9945	12.172	23.909
20	0.0966	0.3644	0.0044	0.9956	8.694	19.562
23	0.0297	0.6227	0.0243	0.9757	19.562	56.511
24	0.0394	0.6227	0.0184	0.9816	19.562	39.123

Figure 6.6 gives us an indication of where to measure the liquid flowrate for a given volume fraction of water.

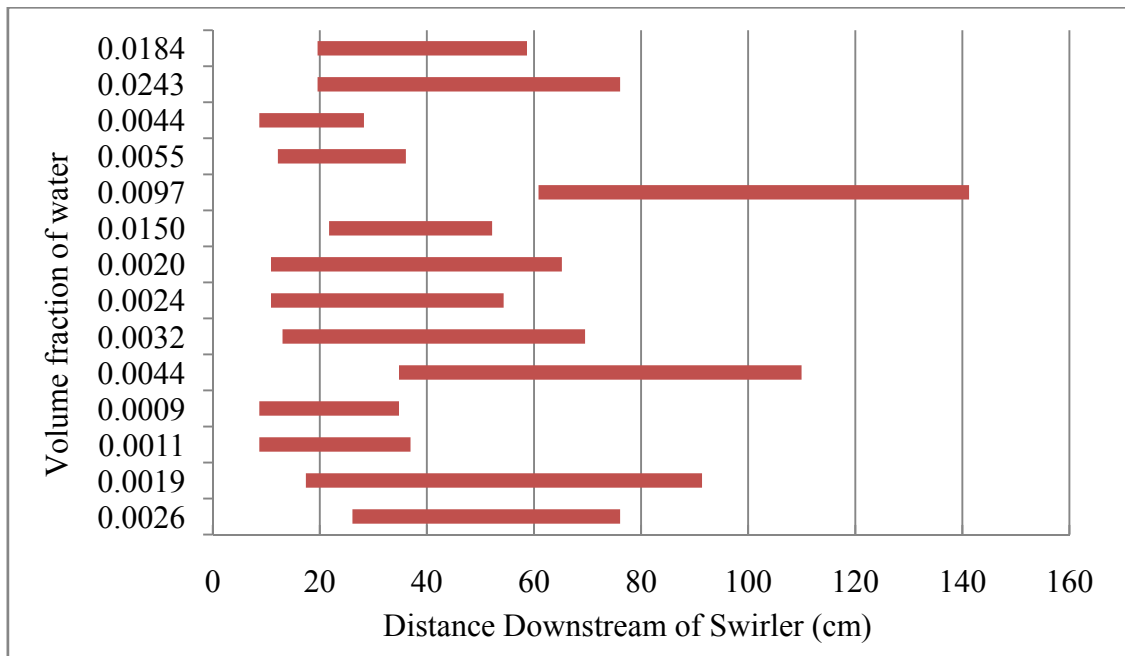


Fig 6.6 - Graph showing range of maximum liquid deposition for a given volume fraction of water

6.1.2. Pressure and Density

In this section, the results obtained from the CFD simulations in terms of pressure, velocity and individual phase velocities are reported, which give an insight into the flow dynamics of swirl flows. In order to maintain uniformity in displaying the results, 5 parallel planes along the length of the pipe (2 before the swirler and 3 after the swirler, as shown in figure 6.7). The Distances of each plane from the inlet are tabulated in table 3. Six lines starting from the center moving towards the periphery along the entire pipe

length (as shown in figure 6.8), and a horizontal plane running through the center of the pipe (as shown in figure 6.9) are used.

Table 6.3 Distances of each plane from the inlet plane

Plane	Distance from inlet(inches)
Inlet	0
1	31.2992
2	62.4803
3	92.0078
4	98.9763
5	107.7165
Outlet	118.1102

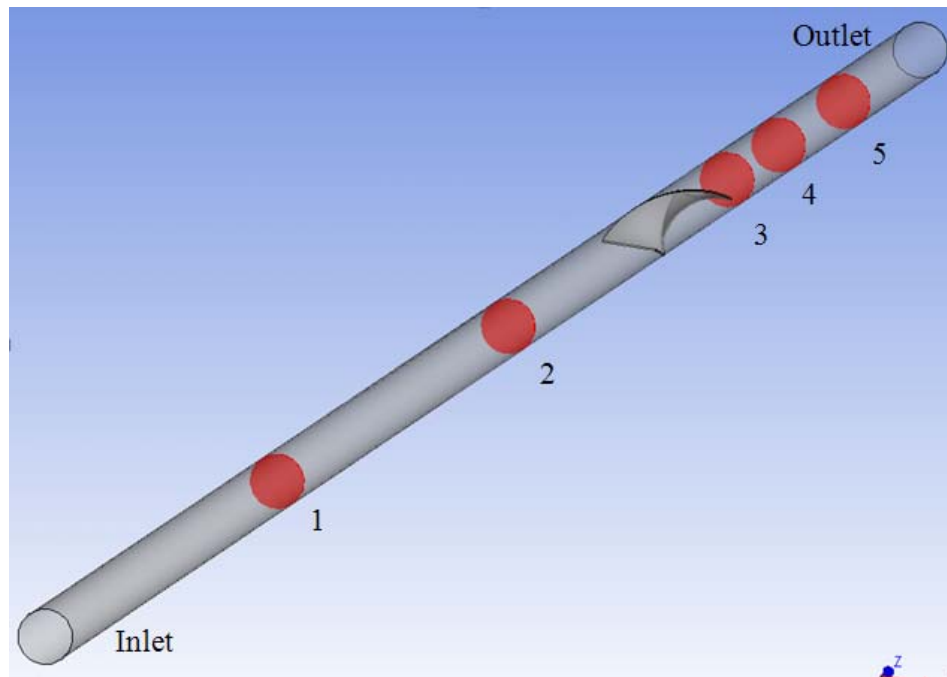


Fig 6.7- 5 sectional planes chosen along the length of the pipe

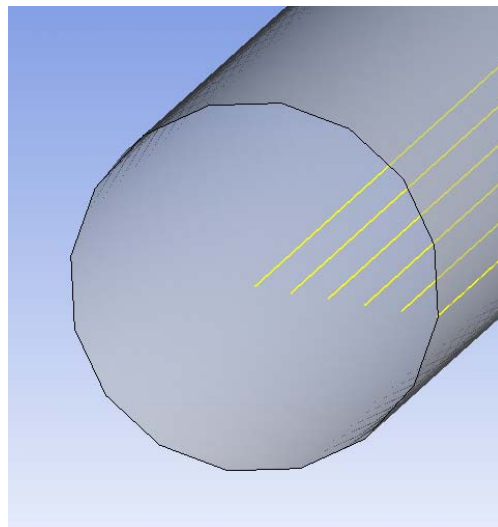


Fig 6.8 - 6 lines chosen along the length of the pipe.

Distance between each line is 2.5mm

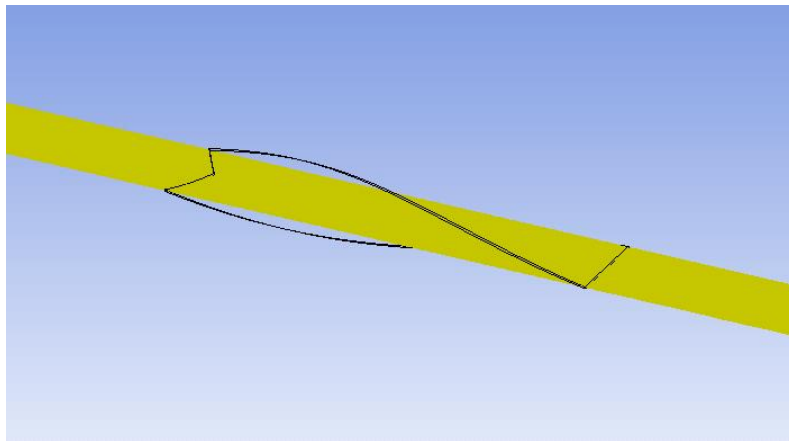


Fig 6.9 - Sectional plane chosen along the length of the pipe

The orientation of plane with reference to the 180 degree twist of the swirl is as shown in figure above. The pressure drop along the pipe is as expected from the experimental data. Figure 6.10 depicts the fluid pressure vs the distance from the pipe inlet along the 5 lines defined earlier.

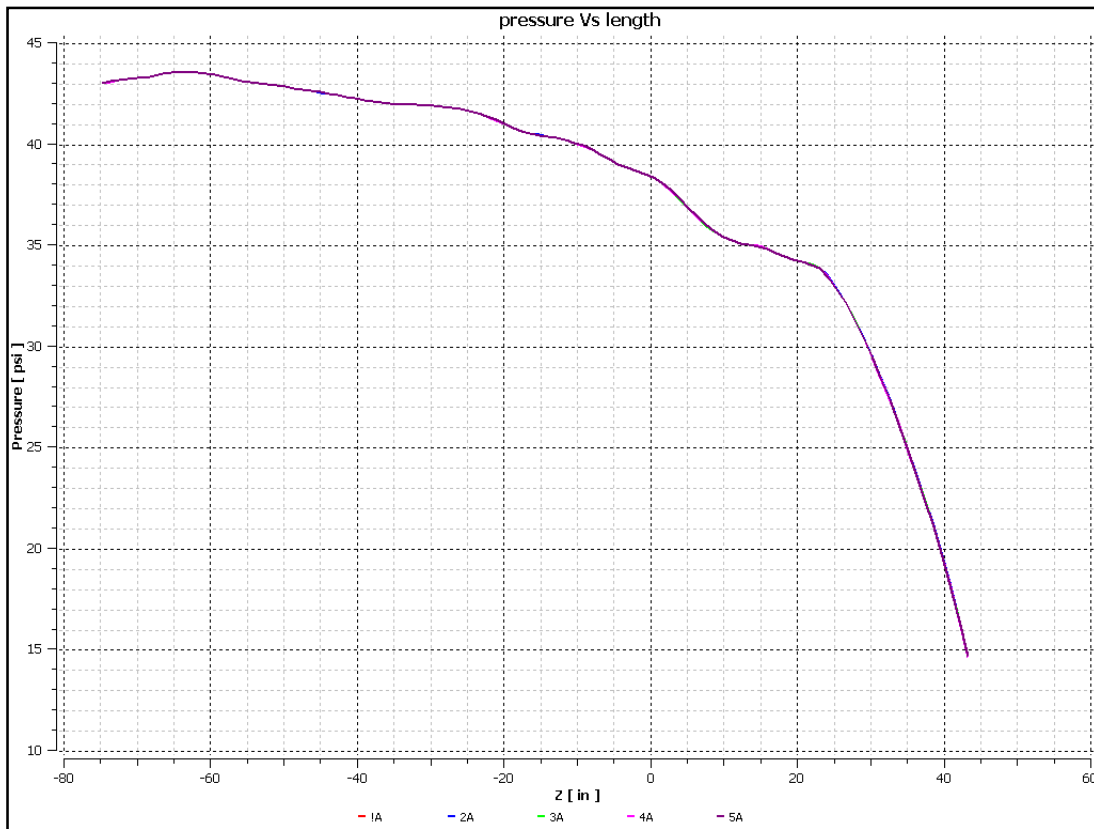


Fig 6.10 - Pressure vs length. All the five lines overlap each other as there is no variation in pressure as we move from center of the pipe to the wall

Figures 6.11 and 6.12 depict the fluid pressure taken at the 5 reference planes and along the horizontal plane that runs through the entire length of the pipe.

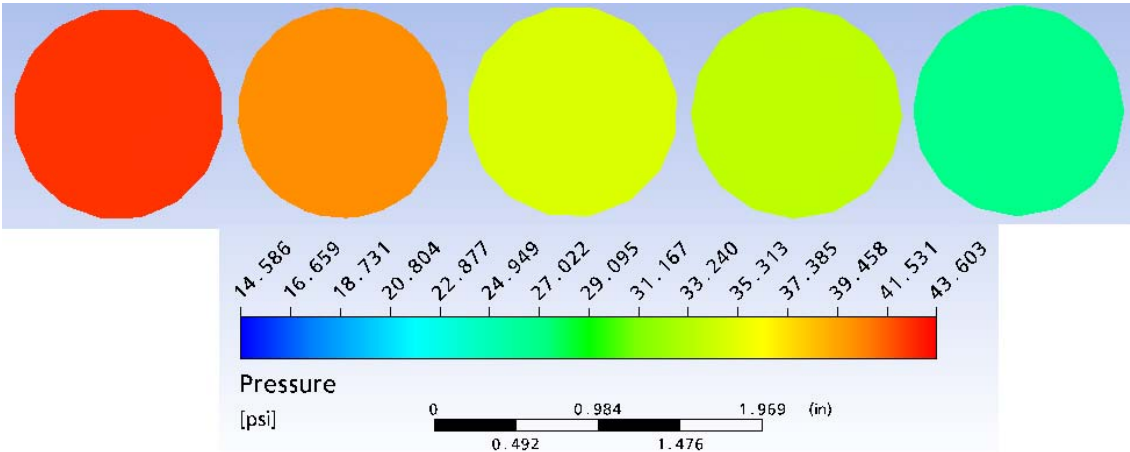


Fig 6.11 –Fluid pressure contours at the 5 cross-sectional planes
(Left to right: plane 1 to plane 5)

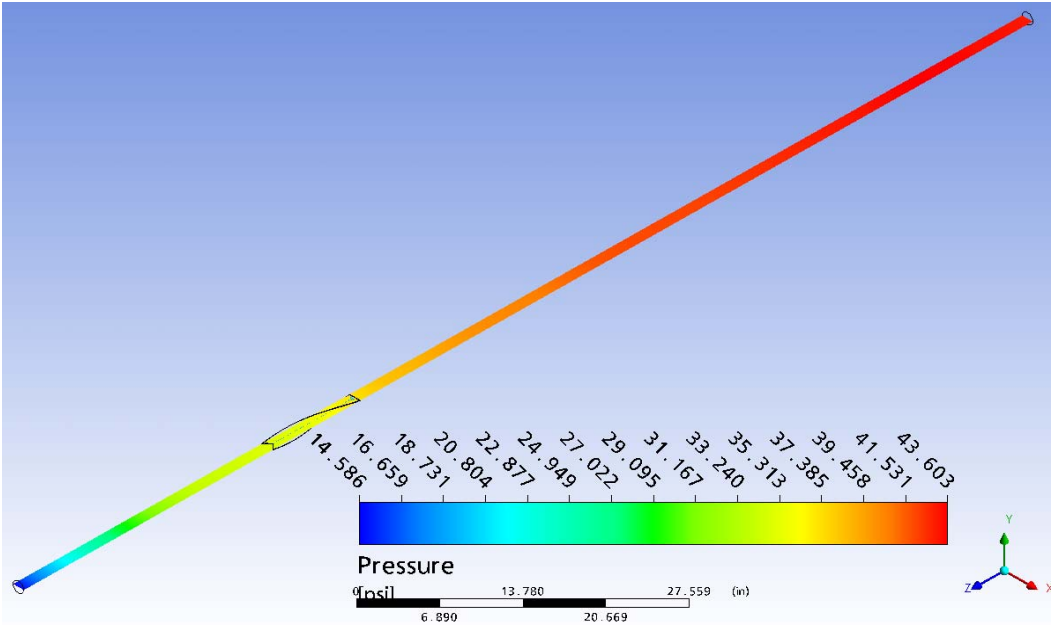


Fig 6.12 - Pressure along the horizontal plane

The following figures depict the changes in density along the 5 planes spanning the length of the pipe. We can see that in planes 3, 4 and 5 the heavier fluid- water is slowly confined to the outer periphery of the pipe. This shows that the swirler separates the two phases and hence creates two distinct flow regions for each of the phases.

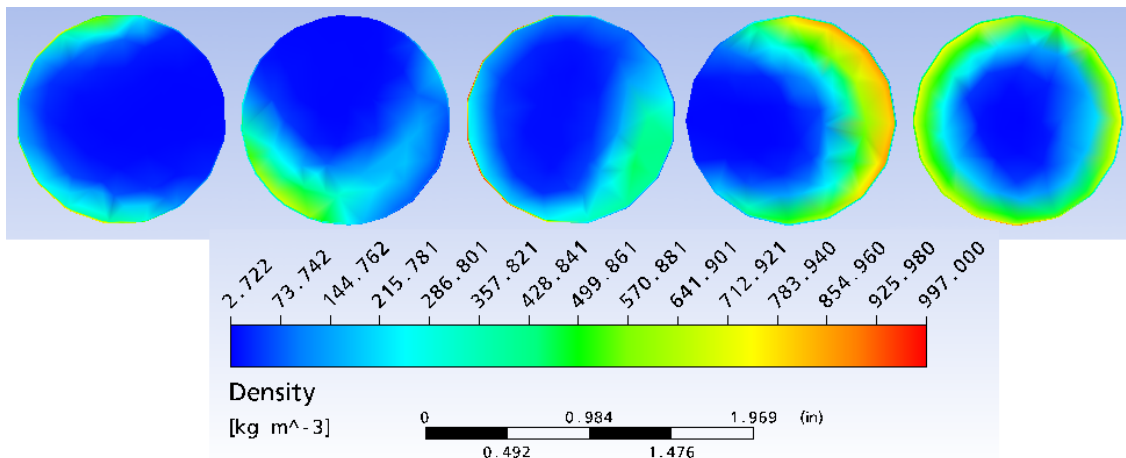


Fig 6.13- Density along the 5 sectional planes

(Left to right: plane 1 to plane 5)

6.2. Liquid Loading

For the liquid loading application, to check if the introduction of the swirler is advantageous or not we concentrate on the superficial velocities of the individual phases. The results have been extracted from the simulations done earlier as a part of ANUMET Validation. The following figures in this section depict the changes in the individual

superficial velocities of each phase. Firstly figure 6.13 and 6.14 depict the changes in the water superficial velocity taken along the 5 sectional planes chosen earlier.

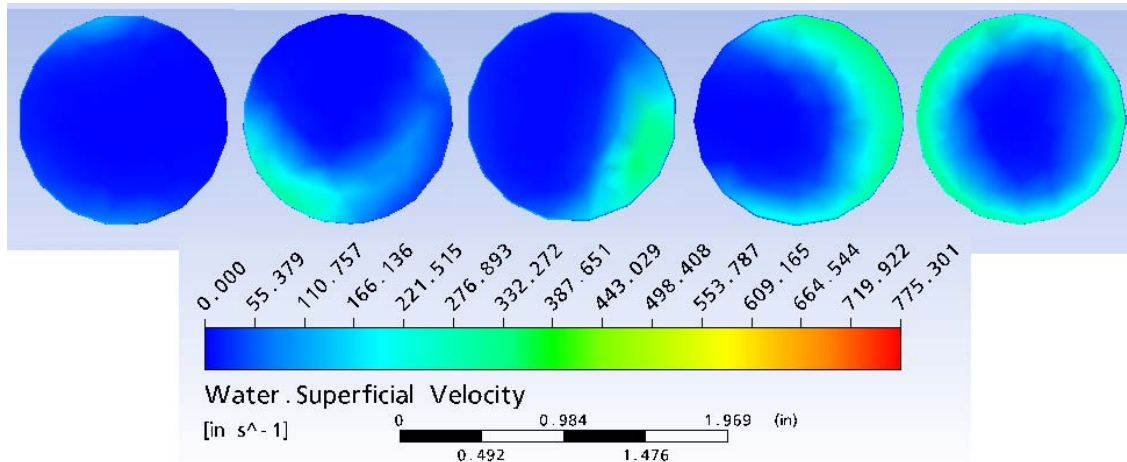


Fig 6.14 – Water superficial velocity on 5 sectional planes
(Left to right: plane 1 to plane 5)

We can clearly see that the water superficial velocity increases gradually and after introduction of swirler the water with higher superficial velocity is confined to the periphery, the same location which is also shown in the density plots with maximum density. This increase has resulted because of introduction of swirler because the gas and water rates are constant and have not been increased or decreased. This is a result of efficient separation of phases by the swirler. By confining the phases to different parts of the pipe (center and periphery) the flow patterns allows this increase in superficial velocities.

Now if we look at the air superficial velocities (figure 6.15) we can observe that a similar but opposite trend to that of the water happens here. The air is confined to the center of the pipe and consequently the superficial velocity of air increases over the span of the pipe.

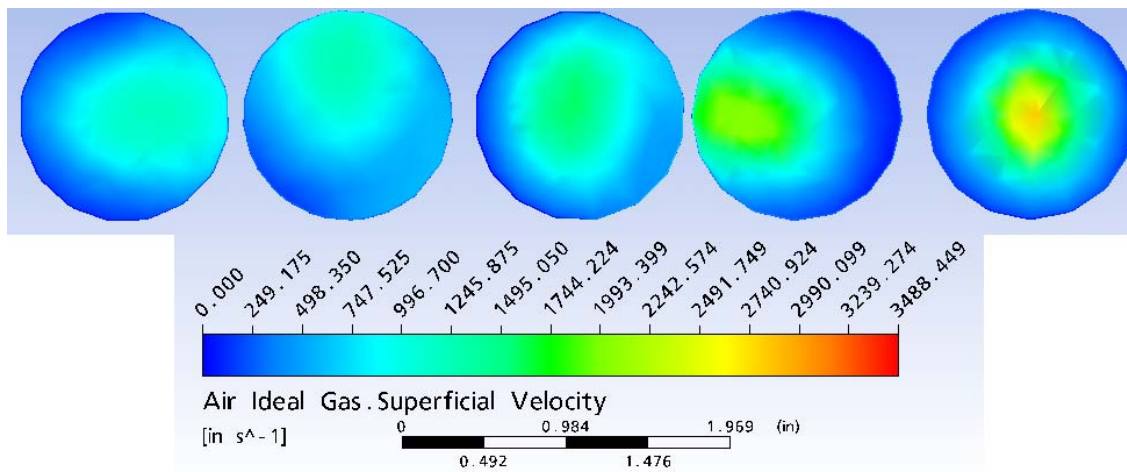


Fig 6.15 - Changes in air superficial velocity along the pipe

(Left to right: plane 1 to plane 5)

These results are particularly important for the liquid loading application. In actuality the liquid loading application would be an upscale version of the ANUMET. In the liquid loading aspect it would be critical to monitor the liquid hold-up parameter. It is defined as the ratio of area occupied by liquid to the total area. Table 4 tabulates the water and gas rates used in the simulations.

Table 6.4 Flow rate data used for simulations in order to check the relation between liquid-hold up and water rate.

RUN	Gas flow rate (Kg/s)	Water flow rate (Kg/s)
1	0.0382	0.0834
2	0.0382	0.222
3	0.0382	0.3644

Figure 6.16 below depicts the water volume fraction up on plane 5 for three increasing water flow rates (left to right). The blue color shows the area occupied by air. So if the area occupied by air is decreasing it means area occupied by water is increasing and hence liquid hold-up.

This means as the water rate increases the liquid hold up is increasing implying that there is more effective liquid removal. Hence we can say that introduction of a swirler does help unload liquids from the wellbore.

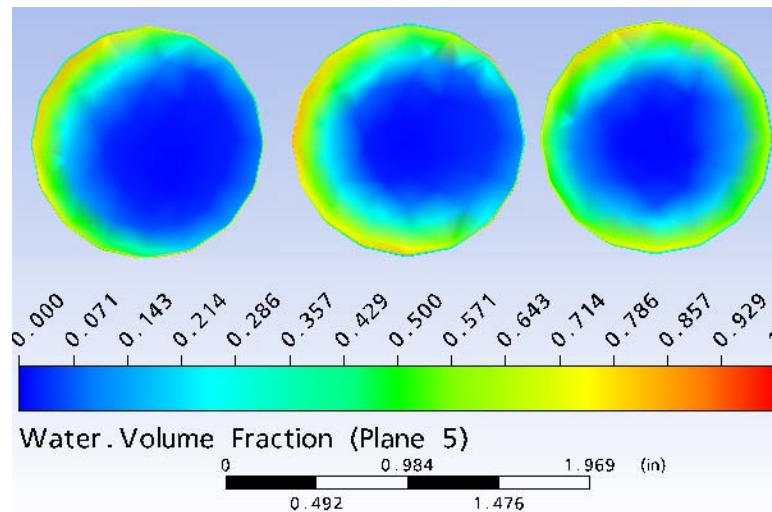


Fig 6.16 - Air superficial velocity along the pipe

(Left to right: run 1 to run 3)

6.3. Erosion at Pipe Bends Due to Sand Transport

The introduction of swirler showed a lot of advantage in this case. Simulations were done on a pipe bend with and without the swirler and the following figures show the erosion rate on the wall when aluminum particles with 0.75 mm diameter which corresponds to coarse sand are suspended in water with a flow rate of 30 kg/s. we can see that the erosion rate has reduced almost 5 times ($7.243 \text{ e}5 / 1.341 \text{ e}5 = 5.4$). This means the life of the pipe has been increased 5 times. This means if the natural life of a pipe is say 10 years with the introduction of a swirler we can increase it to 50 years. The next few figures compare variables like pressure and velocity before and after introduction of swirler.

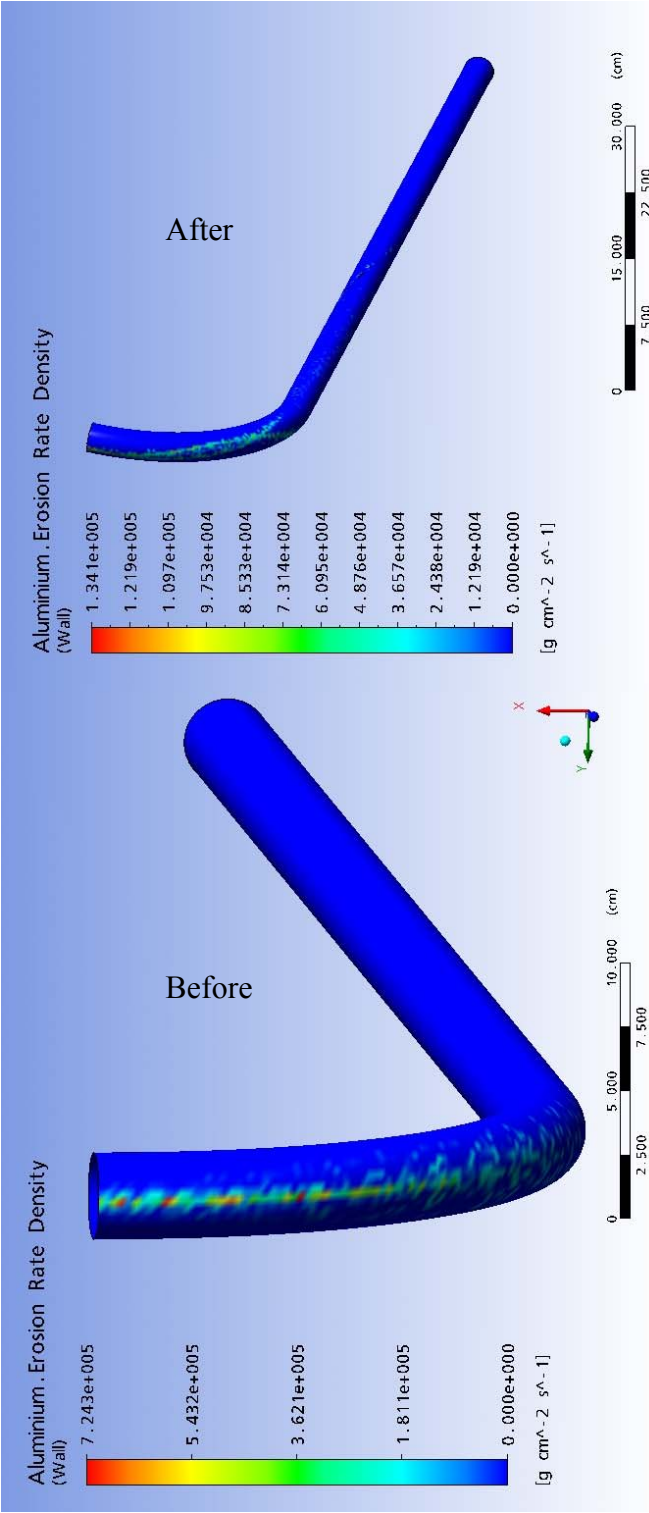


Fig 6.17 - Erosion rate before and after introduction of swirler

6.4. Multiphase Flow Loop

The motive behind setting up the lab was to test two and three phase flow patterns in a transparent section with and without the swirl inducing device. In order to set the flow loop correctly with regards to the right equipment simulations were carried out on just the pipe section with varying pipe diameters (2in, 2.5 in and 3in) to select the correct pipe diameter for the loop. Based on the results from the simulations the 3 inch diameter was selected. The results from these simulations are illustrated in the next 3 figures.

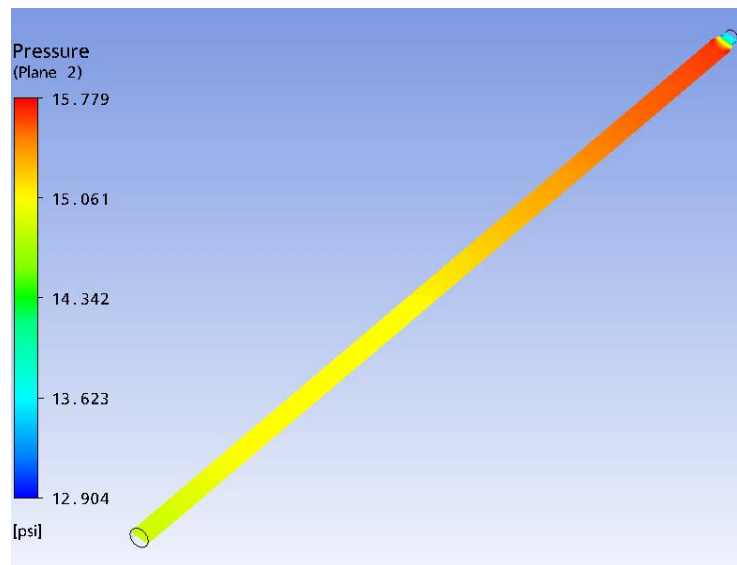


Fig 6.18 - Pressure drop (2.8 psi) in 3 inch diameter pipe

In order to see what is happening inside the pipe, transparent pipe was decided to be used. Out of the 3 diameters investigated only the 2 inch and 3 in were readily available

because the pressure drop in 2 inch diameter pipe was too high it was decided to use the 3 inch diameter for the pipe section. 2 sections of 3in diameter pipe were used to complete the 12 ft of the flow loop.

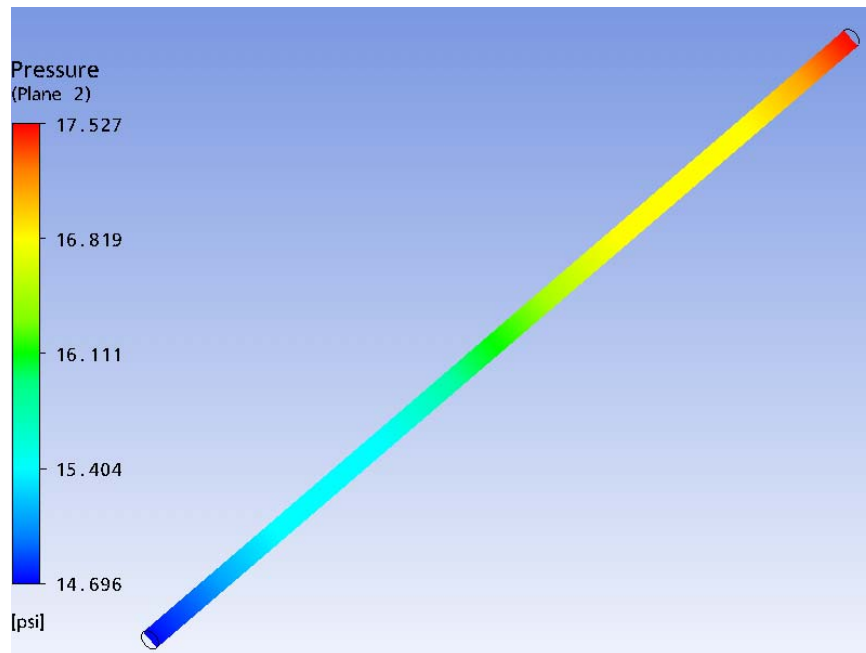


Fig 6.19 - Pressure drop (3 psi) in 2.5 inch diameter pipe

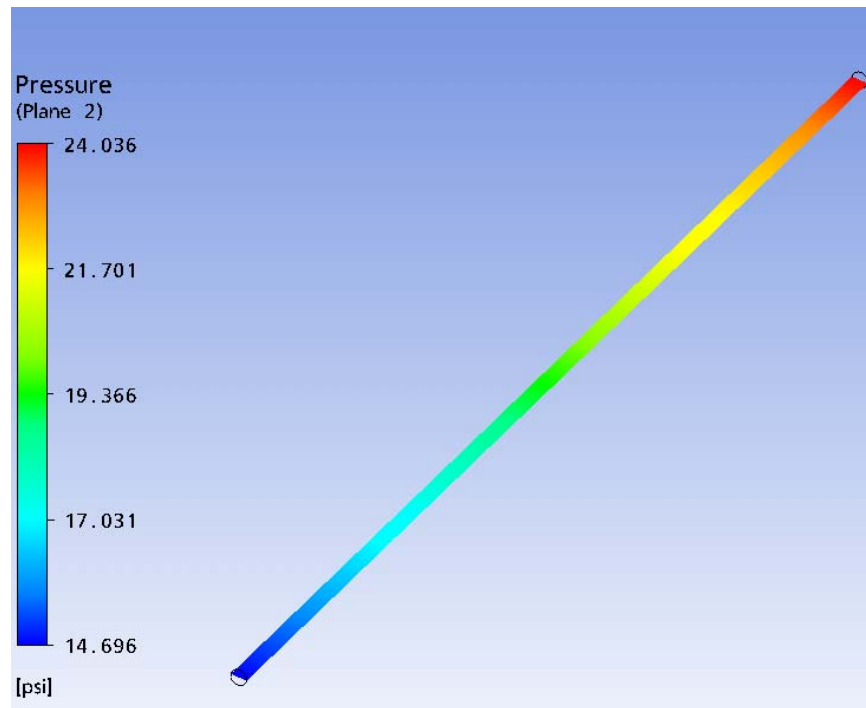


Fig 6.20 - Pressure drop (10 psi) in 2 inch diameter pipe

The following figures describe the flow loop. The flow loop consists of three pipes. Yellow pipe for air which comes in from a compressor located in the basement of the Richardson building and pumps air at 80 psi. The blue flow line is for water and sand which are connected to a multi phase pump. The transparent pipe section is the section where observations and measurements are taken or done.

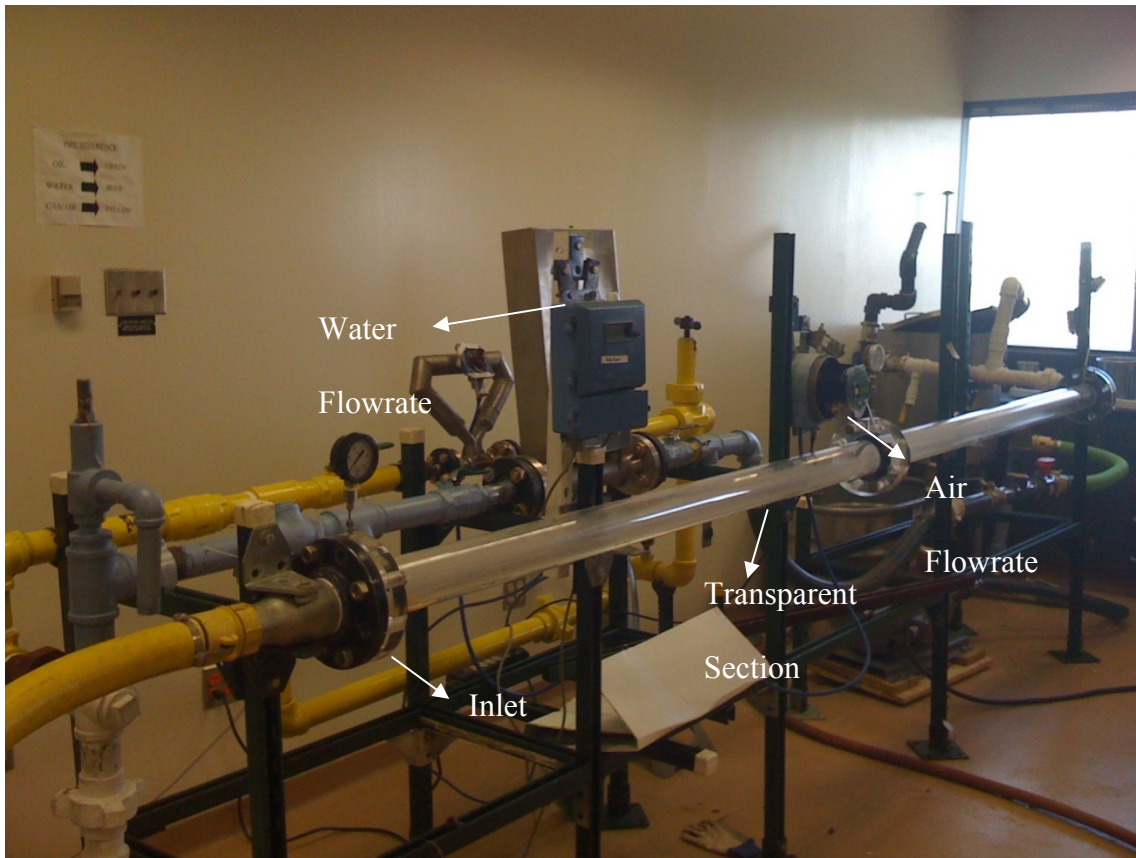


Fig 6.21 - Flow loop

The pressure gauges being used currently are regular analog gauges. The pressure drop along the pipe is very less as this is a horizontal flow line. In order to measure this pressure drop the current pressure gauges do not do a very good job. It would be better if we used pressure transducers and connected that to a data acquisition system.



Fig 6.22 - Instrumentation currently used

The pressure gauges currently being used are very roughly graded with respect to the current application. Finer gauges are required.

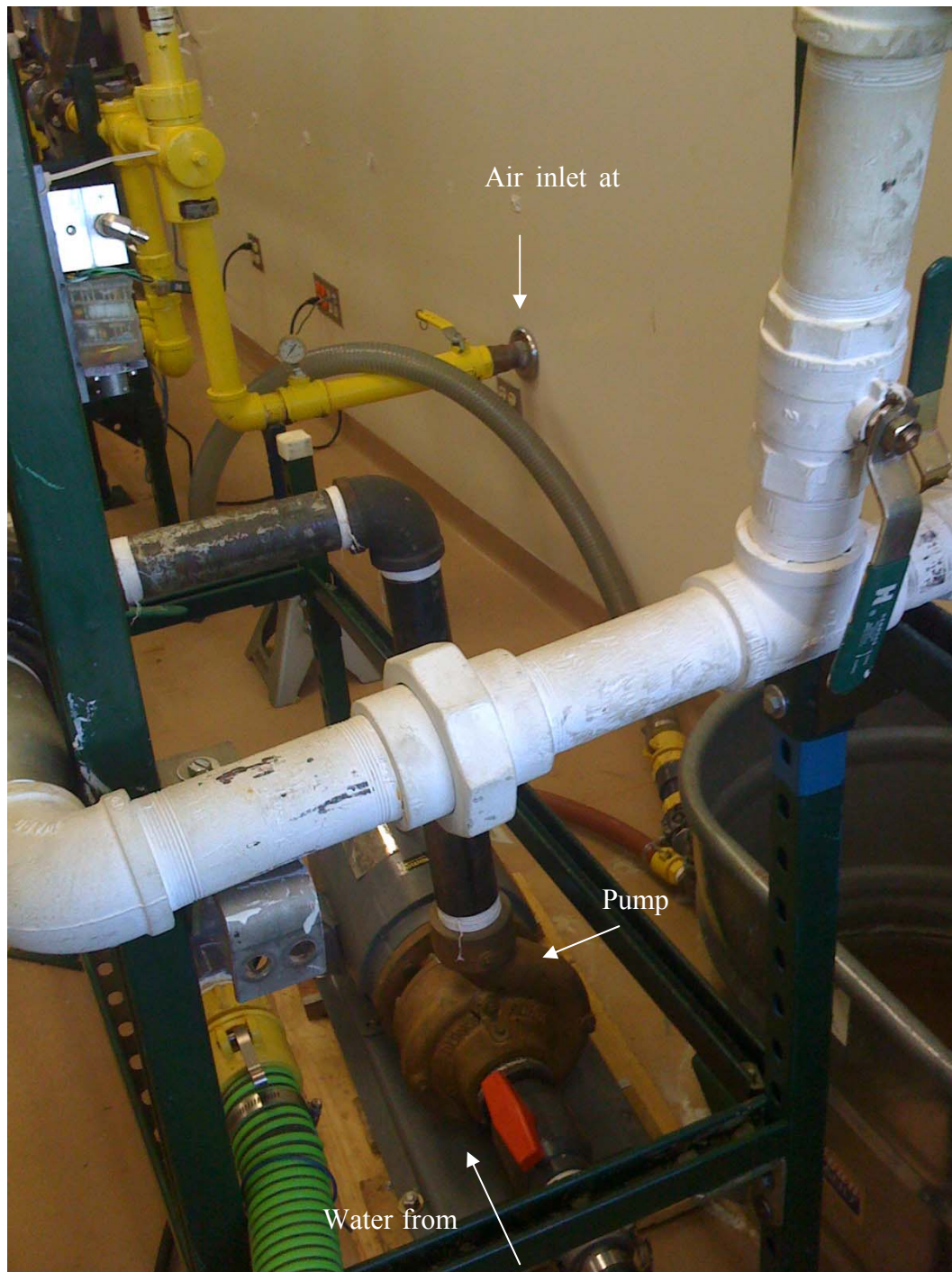


Fig 6.23 - Air and water inlet



Fig 6.24 Water tank

CHAPTER VII

CONCLUSIONS AND RECOMMENDATIONS

This project reviewed the basic principles of swirl flow, with a focus on the swirl effects induced to a two-phase (air-water) flow by a twisted-tape device of the type used in the ANUMET wet gas meter. A commercial CFD software package was used in this study, with the objective of investigating the efficiency of the liquid separation at high gas fraction and evaluating the persistence of the swirl downstream of the flow conditioning device. These features are essential to understand not only the efficiency of in-line separation devices used for wet gas metering purposes, but also that of downhole tools for liquid unloading in gas wells.

The results confirm that the twisted tape induces a swirling motion that results in a separated flow. The liquid flows along the pipe walls, although there remains some entrainment within the gas core. The distribution of the phases across the pipe section is not the same at different locations downstream of the swirler.

For the wet gas metering, a chart was generated from CFD simulations, suggesting the location of maximum liquid deposition downstream of the swirler. This will allow taking pressure and phase fraction measurements (from which the liquid flow rate can be determined) where they are most representative of the flow pattern assumed for the ANUMET calculation algorithms. The experimental data collected by Falcone et al.

(2003) included several test points that were not used in this study and could extend the validity of conclusions obtained from the CFD simulations already presented here.

For the liquid loading application, it was noted that as the water rate increases, the liquid hold-up increases after the fluid passes through the device increased, implying a more effective liquid removal with increasing water rate. Because of limitations in computational power available for this study and modeling capabilities of the selected CFD software package, real field-scale scenarios could not be simulated during this work. In particular, it would be interesting to test the Volume of Fluid (VOF) approach for the liquid loading application. The VOF application is available within other commercially available software.

For the sand erosion application, the CFD simulations indicated that the introduction of a swirler can decrease the erosion rate on the pipe wall and condition the flow. However, this study did not investigate the risk of the swirler itself suffering from erosion and did not attempt to identify the optimum swirler location within the pipe. An extensive literature review performed on this topic, complemented by the CFD simulations, showed the need for a dedicated multiphase test loop for the investigation of sand erosion in horizontal pipes and at bends. The preliminary design of a facility of this type was presented in this work.

NOMENCLATURE

V_z	Average Velocity
F_b	Body Force
β	Constant ,2 nd Phase
P	Density
ρ_p	Density of Particle
D_p	Diameter Of Particle
Eu	Euler Number
G	Gravity
H	Height
$A_{\alpha\beta}$	Interfacial Area
$D_{\alpha\beta}$	Interfacial Length Scale
r	Radius
P	Pressure
Δp	Pressure Drop
M	Momentum
$C_{p\alpha\beta}$	Specific Heat Capacity
V_s	Settling Velocity
F_s	Surface Force
λ	Thermal Conductivity
$\lambda_{\alpha\beta}$	Thermal Conductivity

V	Velocity of particle
U_i	Velocity of phase
μ	Viscosity
R_i	Volume Fraction

REFERENCES

Bose, R. (2007), Unloading Using Auger Tool and Foam and Experimental Identification of Liquid Loading of Low Rate Natural Gas Wells, MS Thesis, Texas A&M University, College Station.

Falcone G., Hewitt, G.F., Lao, L., Richardson, S.M. (2003), ANUMET: A Novel Wet Gas Flowmeter, Paper SPE 84504 presented at the SPE Annual Technical Conference and Exhibition held in Denver, Colorado, 5 – 8 October .

Falcone, G., Teodoriu, C., Reinicke, K.M., Bello, O.O. (2007), Multiphase Flow Modeling Based on Experimental Testing: A Comprehensive Overview of Research Facilities Worldwide and the Need for Future Developments, Paper SPE 110116 presented at the 2007 SPE Annual Technical Conference and Exhibition held in Anaheim, California, 11–14 November .

Hoffmann A.C , Stein L.C (2007), Gas Cyclones and Swirl Tubes-Principles, Design and Operation, location: Springer Verlag.

Jacobsson, S., Austrheim, T., Hoffmann, A.C., (2006), Experimental and Computational Fluid Dynamics Investigation of the Flow in and around Once-Through Swirl Tubes, Industrial & Engineering Chemistry Research. **45**, 6525-6530.

Jones, T.F. (1997), Pipe Design For Improved Particle Distribution And Reduced Wear, European Coal and Steel Community Final Report 7220-EA/841.

Pinheiro da Silva Filho, J.A. (2000), Multiphase Flow Metering with High Gas Content Using Successive Venturi Devices, DIC Thesis, Imperial College, London, U.K.

Raylor, B. (1998), Pipe Design For Improved Particle Distribution and Improved Wear, Ph.D. Thesis, University of Nottingham, Nottingham, U.K.

Scott S.L. , Ahsan J. A., Fehn, B. (2003), Investigation of a New Tool to Unload Liquids from Stripper Gas Wells, paper SPE 84136 presented at the SPE Annual Technical Conference and Exhibition, Denver, 5–8 October.

Spanner, E.F. (1940), British Patent GB521548, 1940.

Spanner, E.F. (1945), British Patent GB569000, 1945.

Wood R.J.K., Jones T.F., Miles N.J., Ganeshalingam J. (2001), Upstream swirl-induction for reduction of erosion damage from slurries in pipeline bends, *Wear* 250 (2001) 770–778.

VITA

Name: Meher Surendra Ravuri Venkata Krishna

Permanent Address: 9100 Westheimer Road, apt 4210
Houston, Texas, 77063

Education: B.Tech, Mechanical Engineering
J.B Institute of Technology & Science – Hyderabad 2006
M.S. Petroleum Engineering
Texas A&M University, College Station 2009

Member: Society of Petroleum Engineers

Email Address: Meher.surendra@gmail.com